Journal Pre-proof

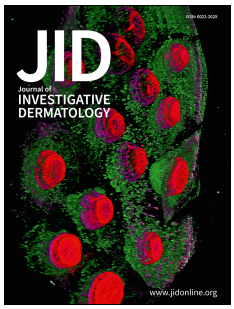

RNA therapy for oncogenic *NRAS*-driven naevi induces apoptosis

Dale Bryant, Sara Barberan-Martin, Ruhina Maeshima, Ignacio del Valle Torres, Mohammad Rabii, William Baird, Aimie Sauvadet, Charalambos Demetriou, Phoebe Jones, Nicole Knöpfel, Fanourios Michailidis, Melissa Riachi, Dorothy C. Bennett, Davide Zecchin, Alan Pittman, Satyamaanasa Polubothu, Stephen Hart, Veronica A. Kinsler

PII: S0022-202X(24)00449-4

DOI: https://doi.org/10.1016/j.jid.2024.04.031

Reference: JID 4305

To appear in: *The Journal of Investigative Dermatology*

Received Date: 10 November 2023

Revised Date: 4 April 2024

Accepted Date: 16 April 2024

Please cite this article as: Bryant D, Barberan-Martin S, Maeshima R, Torres IdV, Rabii M, Baird W, Sauvadet A, Demetriou C, Jones P, Knöpfel N, Michailidis F, Riachi M, Bennett DC, Zecchin D, Pittman A, Polubothu S, Hart S, Kinsler VA, RNA therapy for oncogenic *NRAS*-driven naevi induces apoptosis, *The Journal of Investigative Dermatology* (2024), doi: https://doi.org/10.1016/j.jid.2024.04.031.

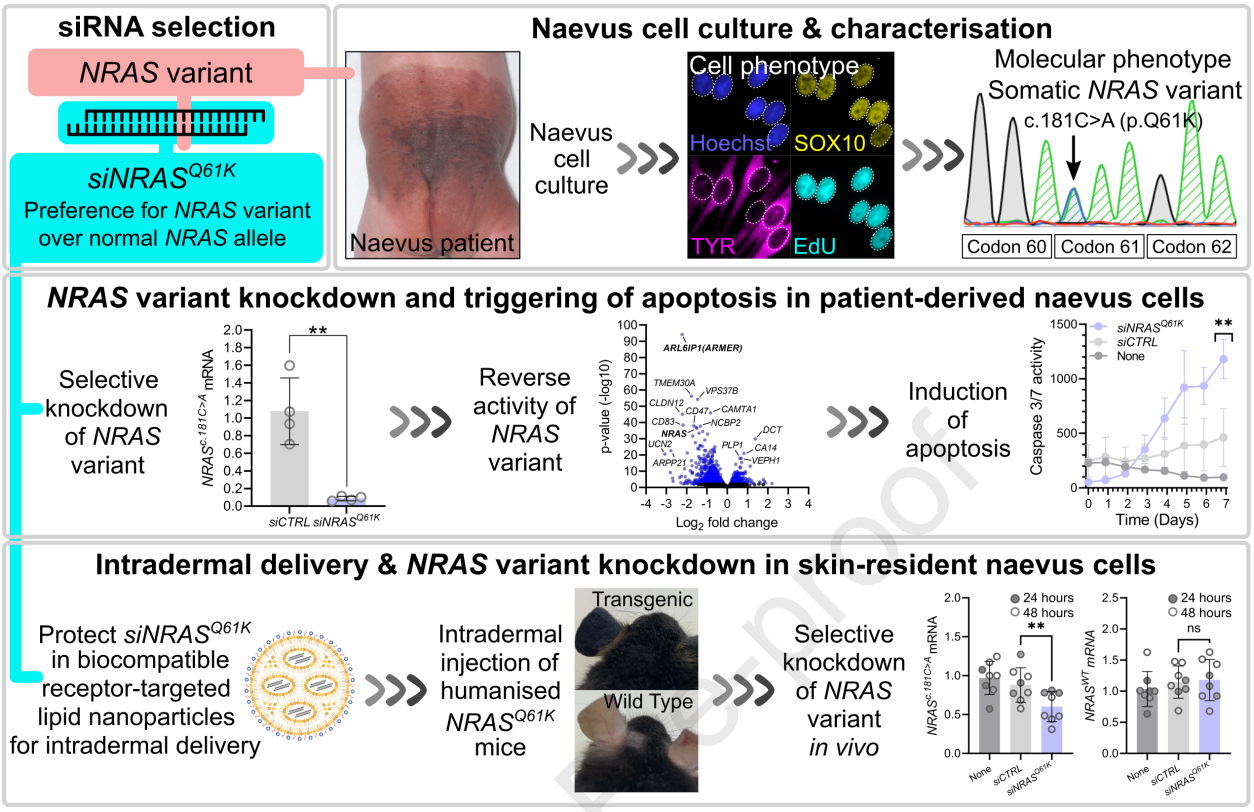

Title

RNA therapy for oncogenic *NRAS*-driven naevi induces apoptosis

Authors

Dale Bryant[1,2], Sara Barberan-Martin[1,2], Ruhina Maeshima[2], Ignacio del Valle Torres[1,2], Mohammad Rabii[1,2], William Baird[2], Aimie Sauvadet[1,2], Charalambos Demetriou[2], Phoebe Jones[1,2], Nicole Knöpfel[1,2,3], Fanourios Michailidis[1,2], Melissa Riachi[1,2], Dorothy C Bennett[4], Davide Zecchin[1,2], Alan Pittman[4], Satyamaanasa Polubothu[1,2,3], Stephen Hart[2], Veronica A. Kinsler[1,2,3]

Affiliations

1. Mosaicism and Precision Medicine Lab, The Francis Crick Institute, London, UK
2. Genetics and Genomic Medicine, UCL GOS Institute of Child Health, London, UK
3. Paediatric Dermatology, Great Ormond Street Hospital for Children, London, UK
4. St George's University of London, London, UK

Corresponding author

Veronica Kinsler, Mosaicism and Precision Medicine Laboratory, The Francis Crick Institute, London, UK; 020 3796 0000; v.kinsler@ucl.ac.uk

Key Words: siRNA, nanoparticle, oncogene, skin, melanocyte

Conflict of interest statement

The authors have declared that no conflict of interest exists. Patent application number GB2216028.7 has been filed in relation to this work on behalf of DB and VK.

ORCiDs

Dale Bryant https://orcid.org/0000-0002-4783-4796

Sara Barberan-Martin https://orcid.org/0000-0003-0142-4078

Ruhina Maeshima https://orcid.org/0000-0003-1473-9757

Ignacio del Valle Torres https://orcid.org/0000-0003-2595-3652

Mohammad Rabii https://orcid.org/0000-0002-1605-6143

William Baird https://orcid.org/0009-0001-7746-7042

Aimie Sauvadet https://orcid.org/0000-0002-8980-1239

Charalambos Demetriou https://orcid.org/0000-0001-6630-1322

Phoebe Jones https://orcid.org/0009-0008-2910-8863

Nicole Knöpfel https://orcid.org/0000-0002-6438-6550

Fanourios Michailidis https://orcid.org/0000-0002-0408-3603

Melissa Riachi https://orcid.org/0000-0001-7278-1780

Dorothy C Bennett https://orcid.org/0000-0002-3639-7527

Davide Zecchin https://orcid.org/0000-0002-4784-0336

Alan Pittman https://orcid.org/0000-0002-8112-2987

Satyamaanasa Polubothu https://orcid.org/0000-0001-7195-5670

Stephen Hart https://orcid.org/0000-0001-8254-376X

Veronica A. Kinsler https://orcid.org/0000-0001-6256-327X

Abstract

RAS proteins regulate cell division, differentiation and apoptosis via multiple downstream effector pathways. Oncogenic RAS variants are the commonest drivers in cancers, however they also drive many benign lesions predisposing to malignancy, such as melanocytic naevi, thyroid nodules, and colonic polyps. Reversal of these benign lesions could reduce cancer incidence, however the effects of oncogenic RAS have been notoriously difficult to target with downstream pathway inhibitors. Here we show effective suppression of oncogenic and currently undruggable *NRAS*^{Q61K} in primary cells from melanocytic naevi using siRNA targeted to the recurrent causal variant. This results in striking reduction in expression of *ARL6IP1*, a known inhibitor of endoplasmic reticulum stress-induced apoptosis not previously linked to NRAS. We go on to show that a single dose of siRNA in primary cells triggers an apoptotic cascade, in contrast to treatment with a MEK inhibitor. Protective packaging of the targeted siRNA into lipid nanoparticles permits successful delivery into a humanised mouse model of melanocytic naevi, and results in variant *NRAS* knockdown *in vivo*. These data show that RAS-induced protection from apoptosis is involved in persistence of *NRAS*-driven melanocytic naevi and anticipate that targeted siRNA could form the basis of clinical trials for RAS-driven benign tumours.

Graphical Abstract

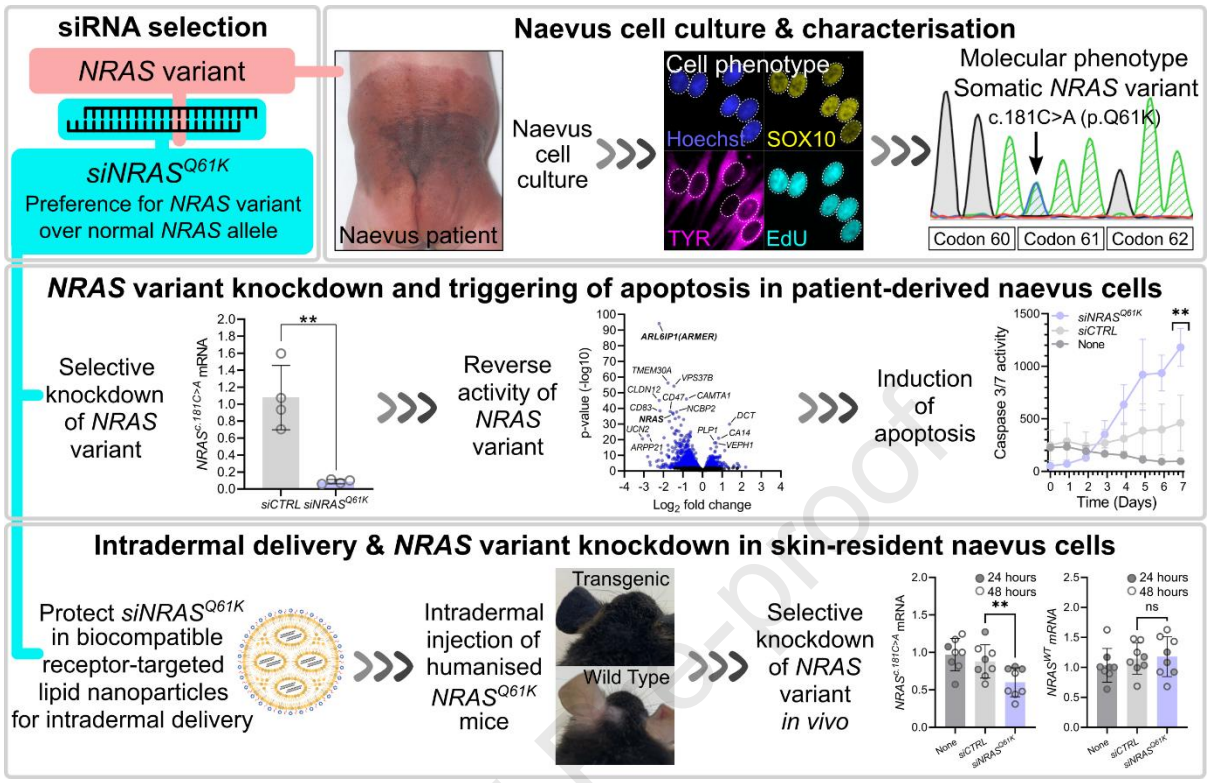

Introduction

The understanding of the role of oncogenic RAS proteins in human health and disease has shifted in recent years. Apart from their established role as cancer drivers, there is increasing evidence of the part they play in clonal expansion within normal tissues and in benign tumours (Dos Santos et al., 2022, Kakiuchi and Ogawa, 2021, Kakiuchi et al., 2020, Marotta et al., 2021, Martincorena et al., 2015, Nanki et al., 2020, Tang et al., 2020, van Laethem, 1999). These insights have highlighted the potential benefits of research into the early origin of RAS-driven cancers, in particular the identification of important downstream biology which might be obscured by subsequent cancer mutations, and the tantalising prospect of preventative therapies. Non-cancer models in which oncogenic RAS can be studied and targeted therapeutically are therefore highly desirable.

The study of congenital human mosaic disorders offers exactly such an opportunity. Mosaic disorders are the result of a single cell mutation during embryogenesis or fetal development (Kinsler et al., 2019), therefore affecting only part of the body. Over the last decade, advanced sequencing techniques comparing clinically affected with unaffected tissues have revealed the causative variants of many of these diseases. These studies have repeatedly uncovered classical oncogenic variants in RAS genes as the monogenic causes, with clinical diseases as distinct as arteriovenous malformations and congenital naevi resulting from the same variants affecting different embryonic cell lineages (Al-Olabi et al., 2018, Bourdeaut et al., 2010, Groesser et al., 2012, Kinsler et al., 2013b). In retrospect their role in these diseases makes perfect sense: these variants govern cell proliferation, differentiation and apoptosis, which are the underlying mechanisms of embryogenesis as much as they are of cancer. It also makes sense of the clinical phenotypes, as many of these mosaic diseases are known to have a cancer predisposition

(Bourdeaut et al., 2010, Hafner et al., 2011, Kinsler et al., 2017a). As the variants are usually incompatible with life in the germline they generally result in sporadic disease, a disease mechanism predicted decades before the variants were found (Happle, 1987).

Congenital melanocytic naevus (CMN) syndrome is a mosaic neurocutaneous disease. The phenotype includes skin lesions from birth that are most easily understood by analogy to acquired melanocytic naevi (AMN). As CMN arise in pre-natal rather than post-natal life however, they differ from AMN in their size, being capable of covering up to 80% of the skin surface (graphical abstract). In AMN the single cell mutation likely affects a specified melanocyte, producing a single naevus. In CMN, the mutation affects a melanocytic precursor at some point in its developmental trajectory and can therefore produce a very broad phenotypic spectrum. This ranges from multiple cutaneous naevi with associated multisystem abnormalities (earlier mutation), to a small single naevus (later mutation). The more severe multiple CMN phenotypes are therefore rarer than the small single naevi, resulting in a continuum of incidence at birth ranging from approximately 1 in 20,000 (Castilla et al., 1981) to 1 in 100 (Alper and Holmes, 1983, Jacobs and Walton, 1976) respectively.

Severe CMN phenotypes are a major source of morbidity and are associated with an increased mortality in childhood. They cause intractable itch, recurrent infections, recurrent development of nodules requiring assessment for malignancy, and difficulties with psychological adjustment in individuals and their families (Masnari et al., 2019). When melanoma dose arise in childhood it is generally rapidly fatal (Kinsler, 2017). Patients are much in need of an effective treatment for their congenital disease, and the promise of such a treatment would bring with it the

prevention of melanoma development, as well as providing proof-of-concept for RAS-driven benign tumour reversal.

CMN is caused in 67% of cases by recurrent oncogenic variants in gene *NRAS*, and the *NRAS* c.181C>A, p.(Q61K) variant is the commonest cause across the whole phenotypic spectrum (Kinsler et al., 2013b, Polubothu et al., 2019). Since the understanding of the genetic causes (Barberan Martin, 2023, Etchevers et al., 2018, Kinsler et al., 2013b, Martins da Silva et al., 2018, Polubothu et al., 2019, Salgado et al., 2015), pathway-targeted cancer therapies have been repurposed as potential treatments for CMN, although oncogenic RAS mutations are notoriously difficult to target with small molecules (Molina-Arcas et al., 2021). The first used was oral MEK inhibitor trametinib for CMN-associated leptomeningeal melanoma, for which there was some benefit in alleviating symptoms before eventual relapse in a case series (Kinsler et al., 2017b, Kusters-Vandevelde et al., 2014), but the CMN themselves remain stubbornly unchanged. Since then, trametinib has also been used successfully to reduce post-natal expansion of nodules in *BRAF*-fusion-CMN (Barberan Martin, 2023, Mir et al., 2019), however again the underlying disease phenotype is unaffected.

These facts led us to conclude that whilst MAPK activation is involved in post-natal proliferations (proliferative nodules and melanoma) and may be important during *in utero* development, the life-long persistence of CMN in the skin is likely not driven by the MAPK pathway. We reasoned that targeting the root cause of the disease, the pathogenic variant itself, would be the best precision medicine approach, and may reveal the downstream pathways of disease persistence. We therefore set out to design targeted genetic therapy for CMN, with a view to testing this in laboratory models. Silencing RNAs targeted specifically at the variant

allele were developed, then incorporated into receptor targeted lipid nanoparticles designed to home preferentially to naevus cells. Targeted silencing was demonstrated in primary patient naevus cells *in vitro*, in patient skin explants, and in a humanised transgenic mouse *in vivo*. Importantly, silencing of the variant allele triggered apoptosis of naevus cells *in vitro*, via a previously unsuspected link to the ER-stress induced apoptosis pathway.

These findings highlight the power of studying oncogenic RAS variants in benign diseases to identify downstream biological pathways and demonstrate proof of concept that such lesions may be reversible. As such this therapeutic approach paves the way not only for potential CMN resolution in humans, but as a potential paradigm for preventative cancer therapies in benign tumours driven by oncogenic RAS.

Results

Design and optimisation of siRNA in HCT116 cells

Variant NRAS c.181C>A transcript expression can be selectively silenced in HCT116 cells

qRT-PCR primers specific to the *NRAS*$^{c.181C>A}$ variant and WT alleles were designed (**Supplementary Table S4**), and specificity confirmed in homozygous *NRAS*$^{c.181C>A}$ HCT116 colorectal carcinoma cell line C6072C (CrownBio) with matched parental wildtype C8052C-WT line (CrownBio). Nineteen 21mer siRNAs were designed by a walked approach spanning the variant of interest (**Figure 1a**). qRT-PCR screening of this panel in the paired HCT116 lines identified three siRNAs (siRNAs 8, 14, 15) which significantly reduced expression of variant (*NRAS*^{Q61K}; $p \leq 0.05$) over WT transcripts (*NRAS*^{WT}; $p > 0.05$) (**Figure 1b**). Allelic discrimination was further assessed using two published formulae (Takahashi and Hohjoh, 2014) (**Figure 1c**). Both identified five siRNAs as likely candidates (siRNA8, 10, 12, 13, 15), all positioning the missense variant within a central window of the siRNA (**Figure 1c**) which was consistent with previous data on siRNA single base targeting (Takahashi and Hohjoh, 2014). siRNAs 8 and 15 were therefore selected for further study, in addition to siRNA1 as an effective silencer of expression of both alleles and therefore a useful control. All three of the selected candidates reduced MAPK pathway activation in *NRAS*$^{c.181C>A}$ mutant HCT116 (**Supplementary Figure S1a**).

siRNA8 has fewest off-target effects on RNAseq in HCT116 cells

Transcriptome-wide RNAseq was undertaken on paired C6072C and C8052C-WT cells with and without treatment with siRNAs 1, 8 and 15, to identify and quantify both on- and off-target effects. Baseline *NRAS* expression levels were lower in the C6072C homozygous variant line (**Figure 1d**) than in the C8052C-WT parent line (**Figure 1e**) for unknown reasons. Variant

NRAS expression by RNA-seq analysis in C6972C cells was silenced to 9%, 79% and 64% of untreated levels by siRNAs 1, 8 and 15 respectively (**Figure 1d**). Variant allele specificity was confirmed for siRNAs 8 and 15 but not siRNA1 as previously demonstrated (**Figure 1d,e**). In contrast to the qPCR data, there was also a small but statistically significant reduction of the *NRAS* WT transcript seen with siRNAs 8 and 15 (**Figure 1e**). siRNA8 alone did not affect the expression of *NRAS* homologues *KRAS* and *HRAS* in non-variant cells (**Supplementary Figure 1b,c**). Expression of genes containing sequences similar to the target sequence of each siRNA were assessed, revealing that siRNA8 had fewer off-target effects compared to siRNA15 (**Supplementary Figure 1d-f**). Pathway analysis of all 2-fold ($p \leq 0.05$) differentially-expressed genes was performed using Metascape (Zhou et al., 2019). siRNA8 had the most limited impact on the transcriptome while maintaining allele specificity and fewest off-target effects (**Figure 1f,g and Supplementary Data 1**).

On this basis siRNA8 was selected as the lead candidate siRNA, henceforth termed *siNRAS*^{Q61K}. Testing of *siNRAS*^{Q61K} then moved from the cancer cell line to primary patient cells. While this removes the possibility of a control population – there are no genetically normal naevus cells – we consider it to be a much more physiological in vitro model: firstly, the cells are heterozygous for the *NRAS*^{Q61K} variant, secondly the cell type is the target of therapy, and lastly, this model introduces physiological inter-sample germline variation which will be the reality in clinical trials.

siRNA knockdown in primary CMN cell cultures

siNRAS^{Q61K} *selectively knocks down expression of the variant transcript in primary CMN cell cultures*

Eight pure primary CMN cell cultures were established (**Figure 2a and Supplementary Figure 2a-d**), and the heterozygous causal variant was confirmed by Sanger sequencing following expansion (**Figure 2b**). Naevus cells (n=4) were treated with a single dose of *siNRAS*^{Q61K} and results analysed at 48 hours. Treatment suppressed the *NRAS* variant allele mRNA levels significantly more than the WT (**Figure 2c-e and Supplementary Figure 2e**). In the absence of an NRAS^{Q61K} specific antibody, total NRAS protein (combined NRAS^{WT} and NRAS^{Q61K}) was demonstrated to be significantly reduced (**Figure 2f,g and Supplementary Figure 2g**).

siNRAS^{Q61K} *does not alter classical melanocytic markers on primary CMN cell cultures*

Baseline characterisation of naevus cells to confirm melanocytic lineage characterised SOX10 and Tyrosinase expression by immunocytochemistry, in addition to MITF, DCT and Nestin (**Supplementary Figure 3a-e**), and markers of senescence P53 (*TP53*) and P16 (*CDKN2A*) (**Supplementary Figure 3f,g**). Despite an increase in *DCT* expression and a small decrease in *NES* expression seen in the RNAseq dataset (**Supplementary Figure 3d,e**), all immunocytochemical markers were unaffected by *siNRAS*^{Q61K} treatment at 48 hours (**Supplementary Figure 3a-g**).

siNRAS^{Q61K} *reduces MAPK pathway activation and proliferation rate in primary CMN cell cultures*

Primary cells from four *NRAS*^{Q61K}-CMN patients were treated with a single dose of *siNRAS*^{Q61K}, after which immunoblotting demonstrated significantly decreased levels of p-ERK/ERK ratio at 48 hours (**Figure 2f,h and Supplementary Figure 2g**). Cells were monitored with EdU incorporation (**Figure 2i**) and live cell imaging (**Figure 2j**) from 24-48 hours post-treatment, revealing reduction in proliferation compared to non-targeting siRNA controls (**Figure 2i,j**), an effect that was dose dependent (**Supplementary Figure 2f**).

siNRAS^{Q61K} reduces the proportion of non-polar cells in primary naevus cell cultures

Label-free ptychographic imaging of naevus cell morphology and behaviour in samples from four patients demonstrated a range of morphologies within each sample (**Supplementary Figure 2b,c**). Morphologies were therefore classified using a machine learning tool, into relative proportions of nonpolar, bipolar, multipolar and large multinucleated likely senescent cells (**Supplementary Figure 4a,b and Supplementary Figure 5**). The fractions of each cell type were consistent between patients (**Supplementary Figure 4d**). The nonpolar morphology generally appeared briefly before a cell division (**Supplementary Figure 4e**), which was notably sometimes into three daughter cells (**Supplementary Figure 4g** and **Supplementary Video 1**). A single dose of *siNRAS^{Q61K}* treatment induced a significant decrease in the fraction of nonpolar cells with no other subtype alterations at 48 hours (**Supplementary Figure 4c**). Flow cytometry based on DNA content (DAPI intensity) analysis did not detect an impact on cell cycle stages following 48 hours of *siNRAS^{Q61K}* treatment (**Supplementary Figure 2k**).

siNRAS^{Q61K} treatment of primary CMN cells suppresses anti-apoptotic marker ARL6IP1

RNAseq was performed on primary naevus cell lines pre- and post-treatment with *siNRAS^{Q61K}* to look for both on- and off-target effects. Expression of variant *NRAS* was significantly and preferentially downregulated over wildtype (**Figure 2e**), whereas highly homologous genes *KRAS* (**Supplementary Figure 2h**) and *HRAS* (**Supplementary Figure 2i**) were unaffected. Pathway analysis of differentially expressed genes identified enrichment primarily for pathways associated with the cell cycle (**Figure 2k, Supplementary Figure 2j and Supplementary Data 2**). The RAL and integrin pathways were also enriched along with pathways associated with neuronal ensheathment (**Figure 2k, Supplementary Figure 2j and Supplementary Data 2**). In contrast, genes associated with melanocyte differentiation were largely unaffected, except for an increase in the expression of *DCT* (**Figure 2k,**

Supplementary Figure 3e). Importantly, the most significantly differentially expressed gene was ADP Ribosylation Factor Like GTPase 6 Interacting Protein 1 or *ARL6IP1*, also known as Apoptosis regulator in the endoplasmic reticulum membrane or *ARMER* (**Figure 2l**).

siNRAS^{Q61K} treatment triggers apoptosis in primary CMN cell cultures

As highlighted above, *ARL6IP1* is highly expressed in naevus cells (**Supplementary Figure 3h**) with a distribution across the endoplasmic reticulum membrane in a pattern similar but not identical to the rough endoplasmic reticulum associated protein Ribophorin 1 (RPN1) (**Figure 3a**). Validation experiments demonstrated that 48 hours of *siNRAS^{Q61K}* treatment results in suppression of *ARL6IP1* gene (**Figure 3b**) and protein (**Figure 3c and Supplementary Figure 3i**) in all patient lines. *ARL6IP1* was also significantly downregulated in the HCT116 cells treated with *siNRAS^{Q61K}* dataset (**Supplementary Figure 6a,b**). *ARL6IP1* is known to have a role in protecting cells from the apoptotic effects of ER stress(Lui et al., 2003) and oncogenic NRAS activity has been demonstrated to drive resistance to ER stress (Bright et al., 2018). We therefore reviewed expression of key ER-stress-induced apoptosis regulators *ERN1, EIF2AK3 (PERK), ATF6, ATF4 and GRP78* (**Supplementary Figure 6)**. *ERN1* and *EIF2AK3(PERK)* were significantly increased on RNAseq (**Supplementary Figure 6d-f**) but only *ERN1* was found to be significantly upregulated in response to *siNRAS^{Q61K}* treatment at 48 hours with qPCR (**Figure 3d and Supplementary Figure 6g**). In parallel we identified a significant reduction *BIRC5* expression with *siNRAS^{Q61K}* treatment in both the naevus cells (**Figure 3e**) and the HCT116 cell datasets (**Supplementary Figure 6c**). *BIRC5* encodes Survivin, a key protein in protection of RAS inducted apoptosis.

Given these early indicators of activation of apoptosis pathways on RNAseq at 48 hours we then measured apoptosis using Caspase3/7 activation in live imaging of cells from 4 naevus

patients over a period of seven days. All naevus cell cultures treated with a single dose of *siNRAS^{Q61K}* showed markedly increased levels over that period in all patients when compared to untreated cells and control siRNA by seven days, emerging from around 3-4 days (**Figure 3f**).

siNRAS^{Q61K} treatment in primary naevus cell cultures permits effectiveness of MEKi

The effectiveness of *siNRAS^{Q61K}* treatment was then compared to that of MEK inhibitor (MEKi) trametinib, currently the only medical therapy to have been tried in CMN patients in vivo. Very few proliferating naevus cells were detected when treated with 5nM trametinib and almost no proliferating cells were detected when treated with 12.5nM trametinib. (**Figure 4a,b**). The effectiveness of *siNRASQ61K* on reducing proliferation was not detected at these concentrations (**Figure 4a,b**). . The effects of combining trametinib and siNRASQ61K on Caspase 3/7 activity were monitored over 5 days as the previous experiment (**Figure 3f**) revealed an effect by that time point. Unlike its effects on proliferation of CMN cells in culture, MEKi trametinib alone had no impact on Caspase 3/7 activity (**Figure 4c,d**). Addition of 12.5nM trametinib to *siNRAS^{Q61K}* treated cells however significantly increased the induction of apoptosis seen with *siNRAS^{Q61K}* treatment alone, an effect not seen with addition of trametinib to *siCTRL* treated cells (**Figure 4c,d**).

Design and testing of receptor-targeted nanoparticles (RTNPs)

Designing a delivery system for siRNA treatment was done with extrapolation to human trials in mind. Whilst we had already incorporated allele-targeting within the siRNA design, additional targeting of the cell type was considered desirable to keep the eventual required dose as low as possible. The KIT receptor was selected as the most melanocyte-specific cell surface

target compared to other skin cells on the basis of single cell expression data (Uhlen et al., 2015), and as a peptide sequence for targeting had already been established in a previous publication (Reshetnyak et al., 2013).

Optimisation of self-assembling receptor-targeted nanoparticles (RTNPs) protects siRNA from degradation and allow delivery into human skin explants

Self-assembling RTNPs have previously been described as highly effective methods of intracellular delivery for siRNA (Tagalakis et al., 2014). Formulation of the RTNPs was optimised using variable peptide content, whilst maintaining equal mass ratios of siRNA and lipid (**Supplementary Figure 7a-c**), producing *siNRAS*^{Q61K}-RTNPs. Mean nanoparticle diameter was assessed using dynamic light scattering at approximately 200nm (**Supplementary Figure 7a,f**). Addition of increasing amounts of peptide altered the lipid nanoparticles from anionic to cationic (**Supplementary Figure 7b**) and in parallel resulted in increased siRNA encapsulation. Encapsulation was complete at ratios 1:3:1 and 1:4:1 (lipid: peptide: siRNA) (**Supplementary Figure 7c**), and protected the siRNA from RNase degradation (**Supplementary Figure 7d**). Treatment of naevus cells with RTNPs containing a peptide sequence reported to bind to the KIT receptor delivered siRNA to the cells (**Supplementary Figure 7g**). *siNRAS*^{Q61K}-RTNPs were successfully delivered to the dermis of CMN patient skin explants after intradermal injection (**Figure 5a,b**).

Treatment with *siNRAS*^{Q61K}-RTNPs in a murine model of CMN

Cy5-siRNA in RTNPs can be delivered successfully into mouse dermis

To demonstrate in vivo delivery, Cy5-tagged control siRNA incorporated into RTNPs was injected into mouse dermis and skin was fixed one hour later. Fluorescence was visualised after

paraffin embedding and H&E staining confirming successful delivery into the dermis (**Supplementary Figure 8c,d**).

Treatment with siNRAS^{Q61K}-RTNPs induces selective knockdown of variant humanised NRAS

Treatment with *siNRAS^{Q61K}*-RTNPs was then tested in a murine model of CMN (*Tg*(*Tyr-NRAS*Q61K*)*1Bee;* MGI:3768645 (Ackermann et al., 2005) (**Supplementary Figure 8a**), in which mice have hyperpigmented skin and an excess of melanin-producing cells present in the dermis (**Figure 5d,e and Supplementary Figure 8b**). Eight mice received two separate intradermal injections of *siNRAS^{Q61K}*-RTNPs into the skin of the back, shaved just prior to the procedure, in addition to an identical neighbouring injection of RTNPs containing non-targeting siRNA as a control. *siNRAS^{Q61K}*-RTNPs induced knockdown of the transgenic variant *NRAS* allele (**Figure 5f**) but not of the WT endogenous *Nras* allele (**Figure 5g**) at 24 and 48 hours. No side effects were observable macroscopically either at the injection site or on mouse behaviour or general health at this time point.

Discussion

Cancer prevention is an area attracting increasing attention and research investment (Cancer Research UK, 2022-2023, Lopez, 2016). Cancer prevention has usually taken the form of lifestyle modifications, such as optimising diet and exercise (Kohler et al., 2016), although notable therapeutic interventions such as eradication of *H. Pylori* to reduce the incidence of gastric cancer have been demonstrated to be effective (Choi et al., 2020). Genetic therapies have not, however, yet been used in the field of cancer prevention. We hypothesised that targeting oncogenic drivers in benign tumours with a predisposition to malignant transformation would not only treat the lesions themselves but serve as proof-of-concept for this therapeutic angle on cancer prevention. We chose to tackle congenital melanocytic naevi

(CMN) as an untreatable benign disease with severe morbidity including progression to fatal childhood melanoma.

The characteristic pathology in this disease is a large number of naevus cells within the dermis which persist throughout life. This is an unusual situation, as melanocytic precursors usually migrate out of the dermis during embryogenesis into the dermal-epidermal junction, where there is thereafter exquisite regulation of numbers and spacing responsible for the uniformity of human skin pigmentation (Nordland et al., 2006). Clinical observations of regrowth of partially resected naevi (Polubothu and Kinsler, 2019) implied that these cells were not persisting due to true senescence. Histological studies instead revealed that they were in a state of extremely low proliferation characterised by stem cell marker expression (Kinsler et al., 2013a), which we considered could be compatible with a RAS-induced quiescence or resistance to apoptosis. Agnostic to the exact mechanisms at the outset, we selected direct targeting of the causative variant as the best potential method to induce resolution of the lesions, and indeed to study the mechanism itself.

Previous reports of *NRAS* knockdown by various RNA interference techniques in cancer cell lines have demonstrated that non-allele-specific targeting reduces proliferation (Burgess et al., 2014) and that targeting of the variant allele as opposed to the wildtype increases apoptosis (Eskandarpour et al., 2005). We demonstrate here that selective silencing of the variant *NRAS* allele is achievable in multiple samples of primary patient cells from benign melanocytic naevi and in skin explants. This leads to a reduction in NRAS protein levels, a downstream reduction in MAPK pathway activation, and a reduction in cellular proliferation rate. Successful protection of the siRNA from degradation and delivery into the dermis, combined with

targeting to naevus cells, then allowed us to deliver this targeted nanomedicine into the skin of a humanised mouse model of CMN, where knockdown was demonstrated at 48 hours after a single treatment.

In terms of mechanism, high baseline levels and significant suppression on siRNA treatment of *ARL6IP1* and *BIRC5* (Survivin) point to induction of apoptosis. ARL6IP1 is located in the membrane of the endoplasmic reticulum (ER) where it protects the cell from apoptosis (Lui et al., 2003) and is important in the survival of tumour cells (Bishayee et al., 2022). Although not known to be downstream of *NRAS*, oncogenic NRAS activity has previously been demonstrated to drive resistance to ER stress (Bright et al., 2018) and inhibition of the MAPK pathway sensitises human melanoma cells to ER stress-induced apoptosis (Jiang et al., 2007). In further support, our transcriptomic data also identified significant upregulation of *ERN1*, a key player in the same pathway. However, expression of other notable genes associated with ER stress (i.e. EIF2AK3, ATF4, ATF6 and GRP78) were unaffected, suggesting that ER stress may not be only reason whereby *siNRAS*^{Q61K} treatment results in the observed apoptosis.

Survivin is known to be highly expressed in cancers and to inhibit activation of caspases (Wheatley and Altieri, 2019). It is downstream of many apoptotic triggers, including ER-stress (Gundamaraju et al., 2018). Expression in non-proliferating adult tissues (which would include congenital melanocytic naevus cells) has traditionally been considered to be very low (Wheatley and Altieri, 2019), however in support of our findings high baseline levels of Survivin have previously been demonstrated in (acquired) melanocytic naevi (Florell et al., 2005). In further support Survivin expression is downstream of oncogenic RAS. With the development of the most targeted small molecule therapy for oncogenic RAS, KRAS^{G12C} inhibitor Sotorasib (Amgen), elevated levels of Survivin were identified as the

mechanism of protection from apoptosis in pancreatic cancer cells (Chang et al., 2023). Our data demonstrating progression from the early induction of these apoptosis markers to high levels of Caspase 3/7 raises the possibility that even transient suppression of variant *NRAS* expression within a disease cell may lead to irreversible triggering of the apoptotic cascade.

The comparison of the effects of treatment with *siNRAS*^{Q61K} and MEKi trametinib alone and in combination is interesting. Whereas trametinib showed reduction in proliferation of CMN cells in culture within 24 hours of treatment, there was no triggering of apoptosis even over a prolonged period when given alone or in combination with control siRNA. However, the addition of trametinib to treatment with targeted siRNA led to a combinatorial effect on both proliferation and induction of apoptosis. While *siNRAS*^{Q61K} is therefore operating via downstream effectors in addition to the MAPK pathway, silencing of the variant allele also appears to permit additional activity of the MEKi.

RNA interference as a therapy has become a reality in clinical practice over the last five years since the first FDA approval in 2018 for Patisiran™ (Alnylam Therapeutics), and the initial concerns about lack of stability of this treatment modality more than refuted by treatments which require only one administration every six months (Ray et al., 2020). Skin disease has not yet been tackled systematically in this way but the findings here strongly support delivery and treatment directly into or onto the skin. Systemic or intrathecal dissemination is likely to be important for targeting of other aspects of the disease and remains to be explored. The use of variant allele specific therapies and receptor targeting add specificity to the treatment which should enable dose minimisation, while the use of lipid nanoparticles appears in these studies to be sufficient to protect the siRNA from degradation in the short term. Backbone

modifications of the siRNA are ongoing to stabilise the therapy without compromising targeting or effectiveness.

Taken together these data show that protection from apoptosis is critically involved in persistence of *NRAS*-driven melanocytic naevi, and that treatment with allele-specific siRNA removes that protection. Reversal of benign RAS driven tumours could potentially form the basis of cancer prevention, particularly in high-risk individuals.

Methods

Patient cohort

CMN naevus cells were cultured from eight children with CMN who had been recruited to research, after written informed consent and under London Bloomsbury Research Ethics Committee approvals 12/LO/1522 and 17/LO/1783, and where *NRAS* c.181C>A p.(Q61K) had been identified on genotyping. Skin samples were obtained either from surgical excision or from punch biopsy. Patient material was handled in compliance with the UK Human Tissue Act and the Declaration of Helsinki.

Culture of HCT116 cell lines

HCT116 colorectal carcinoma WT (CrownBio, C8052C-WT) and homozygous *NRAS*$^{c.181C>A;p.Q61K}$ (CrownBio, C6072C) cells were cultured in McCoy's 5a Medium (ATCC 30-2007) containing 10% fetal bovine serum.

Isolation and culture of primary CMN naevus cells

Skin biopsies were processed in the laboratory within two hours of collection. The hypodermis was removed before the dermis/epidermis was incubated in a solution of PluriSTEM Dispase II (Sigma SCM133) containing 2.5mM calcium chloride dihydrate (Sigma C7902) and 1.5U/ml Collagenase D (Roche 11088858001) at 37°C. Following partial digestion, the epidermis was separated from the dermis with forceps to continue digestion of both components in separate tubes. When the tissues were adequately digested they were resuspended in 5ml Ham F-10 nutrient mix (Thermo Fisher, 11550043) before separation through a 40μm cell strainer (Corning 431750) to remove aggregate material. The cells were pelleted at 250xg for 5 minutes.

The dermis-derived cells and epidermis derived cells were separately resuspended in naevus cell growth medium (**Table S1**). Cells were seeded onto tissue culture treated plastic and media changed every 3-4 days. When cells approached 70-80% confluency they were dissociated with Accutase (Sigma A6964) and reseeded at a lower density. All cultures were incubated in a typical humidified, 37°C, 5% CO_2 incubator.

Live imaging

Cells were seeded into #1.5 high performance cover glass bottomed 24 well plates (Cellvis, P24-1.5H-N) at a density of 5,263 cells per cm^2 (10,000 cells per well) in 500µl media. Imaging was carried out on the Livecyte 2 imaging system (Phasefocus) 24 hours after seeding the cells. The images were acquired with the 10x objective at 10-minute intervals. Images were processed and analysed with Phasefocus Cell Analysis Toolbox software. For the live apoptosis assay, cells were imaged using the Incucyte Live Cell Analysis System. Cells were cultured with 5uM of Caspase 3/7 substrate (Biotium 10402). Measurements were taken every three hours. The first measurement was omitted because condensation disrupted imaging. Analysis was performed using the incucyte's 'basic analyser', from which raw data is exported.

Flow Cytometry

Cells were analysed by flow cytometry using the Amnis ImageStream flow cytometer to analyse the cell cycle based on DNA content (DAPI intensity) and the Aria III cell sorter for measure delivery of siRNA to CMN tissue.

Immunocytochemistry

Naevus cells were washed once with DPBS, fixed with 4% PFA for 20-30 mins at room temperature before washes with DPBS. Cells were incubated in blocking buffer (**Supplementary Table 2**) for 1 hour. They were then incubated with primary antibodies (**Supplementary Table 2**) prepared in blocking buffer. A minimum of 60ul / well of 96 well plate, overnight at 4°C. Following washes in DPBS, the cells were incubated with secondary antibodies (**Supplementary Table 2**) for two hours at room temperature. During the final series of DPBS washes, cells were incubated with 1µg/ml Hoechst 33342 in DPBS.

siRNA design and optimisation

A walked-design panel of 19 21mer (including TT overhang) siRNAs centred on and targeting the variant *NRAS* mRNA transcript (c.181C>A) were custom made from Sigma (**Supplementary Table 3**). ON-TARGETplus non-targeting control pool (Horizon, D-001810-10-50) were used as a scrambled control. siRNAs were optimised using paired parental C8052C-WT and homozygous *NRAS* (c.181C>A; p.Q61K) (C6072C) HCT116 colorectal carcinoma cell line (CrownBio) before testing on naevus cell cultures. Unless otherwise stated cells were transfected by siRNA in their normal media using Lipofectamine® RNAiMAX (ThermoFisher, 13778075) according to the manufacturer's instructions.

In silico evaluation of allelic discrimination

Two formulae were used to assess siRNA candidates for likely allelic discrimination, one tolerating the targeting of the non-target allele and the other not, as per previously published methods(Takahashi and Hohjoh, 2014).

Quantitative PCR

RNA was extracted (Qiagen 74134) and cDNA was synthesised (Applied Biosystems 4368814). Reactions were set up using PowerUP SYBR Green Master Mix (Applied Biosystems A25742) or Taqman Universal PCR Master Mix (Applied Biosystems 4304437) according to the manufacturer's formulation with appropriate primers/Taqman assays (**Supplementary Table 4**). The qPCR protocol was initiated with 50°C for 2 mins and 95°C for 10 mins, followed by 40 cycles of 95°C for 15 seconds and 60°C for 1 min. The qPCR was performed using the QuantStudio 7 Flex Real-Time PCR System (Applied Biosystems). Relative expression values ($2^{-\Delta\Delta Ct}$) were calculated with normalisation to *GAPDH* expression. Data presented in figures is normalised to the mean value of untreated cells / tissue.

Western blot

Protein was extracted in lysis buffer (150mM NaCl, 1% Triton X-100, 50mM Tris pH8, 1µM phenylmethylsulfonyl fluoride, 1x protease inhibitor cocktail (Roche 11836153001), 1x phosphatase inhibitor cocktail (Roche 04906837001)). Protein was prepared in Laemmli buffer containing 12.5mM dithiothreitol before denaturation at 90°C for 10 minutes. Sample was loaded into Mini-PROTEAN TGX gels and run at 100V until proteins of interest were appropriately resolved. Protein was transferred onto Immobolin-FL Transfer Membrane (Merck IPFL00005) with Towbin Buffer (25mM Tris, 192mM Glycine, 20% methanol) using StandardSD Bio-Rad protocol (25V-1A-30mins) on the Trans-Blot Turbo Transfer System (Bio-Rad). Membranes were blocked for 1 hour in appropriate buffers for antibody / imaging method (**Supplementary Table 5**). Primary antibodies were incubated with the membrane in the blocking buffer overnight at 4°C with agitation. Secondary antibodies were incubated with the membrane for 2 hours at room temperature with agitation. Blots were imaged with Clarity Western ECL substrate (Bio-Rad 170-5060) using Gel Doc System (Bio-Rad) for HRP

conjugated secondary antibodies or the Odyssey CLx (LI-COR biosciences) for IRDye conjugated secondary antibodies (**Supplementary Table 5**). The intensity of protein bands was quantified using the gel analysis tool on FIJI. Protein levels were normalised to Vinculin.

Receptor-targeted lipid nanoparticles

Lipids for cationic nanoparticles are resuspended and mixed to a total lipid concentration of 1mg/ml in 100% ethanol: 49.5% Cationic lipid DOTMA (DOTMA 1,2-di-O-octadecenyl-3-trimethylammonium propane (chloride salt). Molecular Weight: 670.575 [CAS: 104872-42-6; Avanti SKU: 890898P]). 49.5% Neutral lipid DOPE (18:1 (Δ9-Cis) PE (DOPE) 1,2-dioleoyl-sn-glycero-3-phosphoethanolamine. Molecular Weight: 744.034 [CAS:4004-05-1; Avanti SKU: 850725P]). 1% PEGylated lipid (DPPE-PEG(2000)Azide 1,2-dipalmitoyl-sn-glycero-3-phosphoethanolamine-N-azido(polyethylene glycol)-2000 (ammonium salt). Molecular Weight: 2760.38 [CAS: Not available; Avanti SKU: 880231P]). Peptide (27 amino acids, Lys-Lys-Lys-Lys-Lys-Lys-Lys-Lys-Lys-Lys-Lys-Lys-Lys-Lys-Lys-Lys-Lys-Gly-Ala-Cys-Ile-Ser-Val-Tyr-Met-Met-Cys-Gly (KKKKKKKKKKKKKKKKKGACISVYMMCG) [AMSBIO, custom request]) is resuspended to a concentration of 10mg/ml in 95% ethanol.

Self-assembly of lipid nanoparticles is initiated by mixing the lipids, peptide and siRNA, in that order and unless otherwise specified at a ratio of 1 : 4 : 1 (lipid : peptide : siRNA). 3 volumes of water must be used for every 1 volume of ethanol (i.e. input of siRNA must be in 3 volumes of water for every 1 volume of ethanol from the lipid and peptide stock). The lipid nanoparticles containing siRNA were dialysed (GeBaFlex-tube – Dialysis kit MWCO 8kDa, Generon) to exchange the ethanol to water, changing the water 3 times over 24 h.

The RTNPs were concentrated by loading the dialysed sample in Centrifugal filter units, (Amicron Ultra, Merck). and centrifugation at speed/time outlined in protocol. The

concentrated nanoparticles were resuspended in sucrose solution (275-300mOsm). Sterile filter (Syringe Filter PTFE 25mm 0.2ulm NSTR, Fisher 15141499).

The hydrodynamic size and charge of lipid nanoparticles was measured with the Malvern Zetasizer. RNase protection assay was performed by treating the formulated lipid nanoparticles or siRNA alone with RNase A at 2µg/ml before incubation for either 1, 2 or 4 hours at 37°C. 1ul of RNase inhibitor was added to stop the digestion. The nanoparticles were then lysed with 16.4mM of SDS before running on an agarose gel. The encapsulation assay was performed by loading formulated lipid nanoparticles into an agarose gel and checking for free siRNA following electrophoresis.

Animals

All animal studies were approved by the Francis Crick Institute's Animal Welfare and Ethical Review Body and licensed under UK Home Office regulations. Tyr::NRASQ61K mice (*Tg*(*Tyr-NRAS*Q61K*)*1Bee;* MGI:3768645; Ackermann et al., 2005) were supplied from the European Mouse Mutant Archive. GM Testing on rederived progeny showed close to inbred and a mix of background strain groups C57BL/6 and the substrains C57BL/6J, C57BL/6JOlaHsd. Secondary background of DBA/2 also detected. Mouse phenotype and health was consistent with previous published reports, having uniformly black skin including ears, paws and tail. No mouse developed melanoma during the duration of the study.

***In vivo* delivery of lipid nanoparticles to Tyr::*NRAS*Q61K mice**

Tyr::NRASQ61K mice (age = 41–45 weeks, 3x females, 5x males) were shaved with clippers before receiving intradermal injections (insulin needle 30G) of 450µg of RTNPs prepared in

sucrose solution (295 mOsmol) either side of the dorsal midline while under general anaesthesia (isolfurane). Injection sites were marked by drawing around the bleb with a marker pen. 48 hours later the mice were culled and a 4mm punch biopsy was collected from each site. The biopsy was stored in RNAlater (Invitrogen AM7021) prior to RNA extraction.

RNAseq

Two separate RNAseq experiments were run, the first for HCT116 cells and the second for primary naevus cells. HCT116 cells were treated with *siCTRL* (*n*=3), *siRNA1* (*n*=3), *siRNA8* (*n*=3) or *siRNA15* (*n*=3). Patient (*N*=7) naevus cells were each treated with *siCTRL*, *siNRAS*^{Q61K} (*siRNA8*) or no treatment. Total RNA was extracted from cells using the AllPrep DNA/RNA Mini Kit (Qiagen). cDNA libraries were prepared using the KAPA 12 mRNA HyperPrep Kit (Roche) and subsequently sequenced on a NextSeq 500 sequencer 13 (paired-end) (Illumina). Fastq files were processed by fastp (0.20.0) and aligned to the human genome (Ensembl, GRCh 38.109) using STAR (2.7.9a). The uniquely mapped read counts matrix was obtained using featureCounts (Rsubsead 1.6.4) and differential-expression analysis was performed using DESeq2 (1.38.3). Adjusted *p*-values were collected with Benjamini-Hochberg correction. PCA plot was generated using functions included in the same package.

Statistical analysis

Statistical analyses were carried out as described in each figure using either a t-test or ANOVA. Corrections for multiple comparisons (Tukey, Bonferroni or Šidák) were done by selecting the recommended option on GraphPad Prism. Adjusted *p*-values (Benjamini-Hochberg correction) were used with RNAseq data. Non-statistically significant difference = ns $p>0.05$. Statistically significant difference = * $p\leq0.05$ and ** $p\leq0.01$.

Data Availability Statement

Datasets related to this article can be found at ArrayExpress (https://www.ebi.ac.uk/biostudies/arrayexpress), hosted at accession number E-MTAB-13221.

Author contributions

Conceptualisation: VK; Data Curation: IDVT, AP; Formal Analysis: DB, WB, CD, MRa, VK; Funding acquisition: VK; Investigation: DB, SB, MRa, MRi, WB, CD, DZ, FM, PJ, NK, SP; Methodology: SP, DCB, RM, SH, AS; Project administration: VK; Resources: NK, RM, SH; Supervision: SH, VK; Visualisation: DB; Writing – original draft: DB, VK; Writing – review and editing: VK

Acknowledgments

We gratefully acknowledge the participation of the patients and families in this research. We gratefully acknowledge the support and expertise of the UK National Institute of Health and Social Care (NIHR) grant steering committee: Jane White (UCL/Crick - Chair), Prof Lionel Larue (Curie Institute), Prof Gudrun Moore (University College London), Prof Nick Reynolds (Newcastle University) and Prof Francesco Muntoni (University College London). VK and DB are funded by a NIHR Research Professorship (grant NIHR300774). This project was supported by the NIHR (grant NIHR300774), Caring Matters Now Charity, and the LifeArc-Crick Fund. The work was supported by the GOSHCC Livingstone Skin Research Centre and by the UK NIHR through the Biomedical Research Centre at Great Ormond St Hospital for Children NHS Foundation Trust and the UCL GOS Institute of Child Health. Research support was provided by the Crick Science Technology Platforms: Advanced Light Microscopy, Advanced Sequencing, Biological Research Facility, Experimental Histopathology, Flow Cytometry, High Throughput Screening and Structural Biology.

References

Ackermann J, Frutschi M, Kaloulis K, McKee T, Trumpp A, Beermann F. Metastasizing melanoma formation caused by expression of activated N-RasQ61K on an INK4a-deficient background. Cancer research 2005;65(10):4005-11.

Al-Olabi L, Polubothu S, Dowsett K, Andrews KA, Stadnik P, Joseph AP, et al. Mosaic RAS/MAPK variants cause sporadic vascular malformations which respond to targeted therapy. J Clin Invest 2018.

Alper JC, Holmes LB. The incidence and significance of birthmarks in a cohort of 4,641 newborns. Pediatric dermatology 1983;1(1):58-68.

Barberan Martin S, Polubothu S, Bruzos AL, Kelly G, Horswell S, Sauvadet A, Bryant D, Zecchin D, Riachi M, Sadri A, Michailidis F, Muwanga-Nanyonjo N, Lopez-Balboa Pablo, Knoepfel N, Bulstrode N, Pittman A, Yeh, I, Kinsler VA. Mosaic BRAF fusions are a recurrent cause of congenital melanocytic naevi targetable by MEK inhibition. Journal of Investigative Dermatology 2023;Accepted and in press.

Bishayee K, Habib K, Nazim UM, Kang J, Szabo A, Huh SO, et al. RNA binding protein HuD promotes autophagy and tumor stress survival by suppressing mTORC1 activity and augmenting ARL6IP1 levels. J Exp Clin Cancer Res 2022;41(1):18.

Bourdeaut F, Herault A, Gentien D, Pierron G, Ballet S, Reynaud S, et al. Mosaicism for oncogenic G12D KRAS mutation associated with epidermal nevus, polycystic kidneys and rhabdomyosarcoma. Journal of medical genetics 2010;47(12):859-62.

Bright MD, Clarke PA, Workman P, Davies FE. Oncogenic RAC1 and NRAS drive resistance to endoplasmic reticulum stress through MEK/ERK signalling. Cell Signal 2018;44:127-37.

Burgess MR, Hwang E, Firestone AJ, Huang T, Xu J, Zuber J, et al. Preclinical efficacy of MEK inhibition in Nras-mutant AML. Blood 2014;124(26):3947-55.

Cancer Research UK. Cancer Research UK Prevention Research Strategy. 2022-2023.

Castilla EE, da Graca Dutra M, Orioli-Parreiras IM. Epidemiology of congenital pigmented naevi: I. Incidence rates and relative frequencies. The British journal of dermatology 1981;104(3):307-15.

Chang WH, Liu Y, Hammes EA, Bryant KL, Cerione RA, Antonyak MA. Oncogenic RAS promotes MYC protein stability by upregulating the expression of the inhibitor of apoptosis protein family member Survivin. J Biol Chem 2023;299(2):102842.

Choi IJ, Kim CG, Lee JY, Kim YI, Kook MC, Park B, et al. Family History of Gastric Cancer and Helicobacter pylori Treatment. The New England journal of medicine 2020;382(5):427-36.

Dos Santos W, Dos Reis MB, Porto J, de Carvalho AC, Matsushita M, Oliveira G, et al. Somatic targeted mutation profiling of colorectal cancer precursor lesions. BMC Med Genomics 2022;15(1):143.

Eskandarpour M, Kiaii S, Zhu C, Castro J, Sakko AJ, Hansson J. Suppression of oncogenic NRAS by RNA interference induces apoptosis of human melanoma cells. International journal of cancer Journal international du cancer 2005;115(1):65-73.

Etchevers HC, Rose C, Kahle B, Vorbringer H, Fina F, Heux P, et al. Giant congenital melanocytic nevus with vascular malformation and epidermal cysts associated with a somatic activating mutation in BRAF. Pigment cell & melanoma research 2018.

Florell SR, Bowen AR, Hanks AN, Murphy KJ, Grossman D. Proliferation, apoptosis, and survivin expression in a spectrum of melanocytic nevi. Journal of cutaneous pathology 2005;32(1):45-9.

Groesser L, Herschberger E, Ruetten A, Ruivenkamp C, Lopriore E, Zutt M, et al. Postzygotic HRAS and KRAS mutations cause nevus sebaceous and Schimmelpenning syndrome. Nature genetics 2012;44(7):783-7.

Gundamaraju R, Vemuri R, Chong WC, Myers S, Norouzi S, Shastri MD, et al. Interplay between Endoplasmic Reticular Stress and Survivin in Colonic Epithelial Cells. Cells 2018;7(10).

Hafner C, Toll A, Real FX. HRAS mutation mosaicism causing urothelial cancer and epidermal nevus. The New England journal of medicine 2011;365(20):1940-2.

Happle R. Lethal genes surviving by mosaicism: a possible explanation for sporadic birth defects involving the skin. Journal of the American Academy of Dermatology 1987;16(4):899-906.

Jacobs AH, Walton RG. The incidence of birthmarks in the neonate. Pediatrics 1976;58(2):218-22.

Jiang CC, Chen LH, Gillespie S, Wang YF, Kiejda KA, Zhang XD, et al. Inhibition of MEK sensitizes human melanoma cells to endoplasmic reticulum stress-induced apoptosis. Cancer Res 2007;67(20):9750-61.

Kakiuchi N, Ogawa S. Clonal expansion in non-cancer tissues. Nat Rev Cancer 2021;21(4):239-56.

Kakiuchi N, Yoshida K, Uchino M, Kihara T, Akaki K, Inoue Y, et al. Frequent mutations that converge on the NFKBIZ pathway in ulcerative colitis. Nature 2020;577(7789):260-5.

Kinsler V, A, O'Hare P, Bulstrode N, Chong WK, Sebire N,J, Hargrave D, Slater O. Melanoma in congenital melanocytic naevi. British Journal of Dermatology 2017;In press.

Kinsler VA, Anderson G, Latimer B, Natarajan D, Healy E, Moore GE, et al. Immunohistochemical and ultrastructural features of congenital melanocytic naevus cells support a stem-cell phenotype. The British journal of dermatology 2013a;169(2):374-83.

Kinsler VA, Boccara O, Fraitag S, Torrelo A, Vabres P, Diociauti A. Mosaic abnormalities of the skin - review and guidelines from the European Reference Network for rare skin diseases (ERN-Skin). The British journal of dermatology 2019.

Kinsler VA, O'Hare P, Bulstrode N, Calonje JE, Chong WK, Hargrave D, et al. Melanoma in congenital melanocytic naevi. The British journal of dermatology 2017a;176(5):1131-43.

Kinsler VA, O'Hare P, Jacques T, Hargrave D, Slater O. MEK inhibition appears to improve symptom control in primary NRAS-driven CNS melanoma in children. British journal of cancer 2017b;116(8):990-3.

Kinsler VA, Thomas AC, Ishida M, Bulstrode NW, Loughlin S, Hing S, et al. Multiple congenital melanocytic nevi and neurocutaneous melanosis are caused by postzygotic mutations in codon 61 of NRAS. The Journal of investigative dermatology 2013b;133(9):2229-36.

Kohler LN, Garcia DO, Harris RB, Oren E, Roe DJ, Jacobs ET. Adherence to Diet and Physical Activity Cancer Prevention Guidelines and Cancer Outcomes: A Systematic Review. Cancer epidemiology, biomarkers & prevention : a publication of the American Association for Cancer Research, cosponsored by the American Society of Preventive Oncology 2016;25(7):1018-28.

Kusters-Vandevelde HV, Willemsen AE, Groenen PJ, Kusters B, Lammens M, Wesseling P, et al. Experimental treatment of NRAS-mutated neurocutaneous melanocytosis with MEK162, a MEK-inhibitor. Acta neuropathologica communications 2014;2:41.

Lopez G. Investing in Cancer Prevention and Control to Reduce Global Economic Burden. 2016.

Lui HM, Chen J, Wang L, Naumovski L. ARMER, apoptotic regulator in the membrane of the endoplasmic reticulum, a novel inhibitor of apoptosis. Mol Cancer Res 2003;1(7):508-18.

Marotta V, Bifulco M, Vitale M. Significance of RAS Mutations in Thyroid Benign Nodules and Non-Medullary Thyroid Cancer. Cancers (Basel) 2021;13(15).

Martincorena I, Roshan A, Gerstung M, Ellis P, Van Loo P, McLaren S, et al. Tumor evolution. High burden and pervasive positive selection of somatic mutations in normal human skin. Science 2015;348(6237):880-6.

Martins da Silva V, Martinez-Barrios E, Tell-Marti G, Dabad M, Carrera C, Aguilera P, et al. Genetic Abnormalities in Large to Giant Congenital Nevi: Beyond NRAS mutations. The Journal of investigative dermatology 2018.

Masnari O, Neuhaus K, Aegerter T, Reynolds S, Schiestl CM, Landolt MA. Predictors of Health-related Quality of Life and Psychological Adjustment in Children and Adolescents With Congenital Melanocytic Nevi: Analysis of Parent Reports. J Pediatr Psychol 2019;44(6):714-25.

Mir A, Agim NG, Kane AA, Josephs SC, Park JY, Ludwig K. Giant Congenital Melanocytic Nevus Treated With Trametinib. Pediatrics 2019;143(3).

Molina-Arcas M, Samani A, Downward J. Drugging the Undruggable: Advances on RAS Targeting in Cancer. Genes (Basel) 2021;12(6).

Nanki K, Fujii M, Shimokawa M, Matano M, Nishikori S, Date S, et al. Somatic inflammatory gene mutations in human ulcerative colitis epithelium. Nature 2020;577(7789):254-9.

Nordlund JJ, Boissy, R.E., Hearing, V.J., King, T.A., Oetting, W.S., Ortonne, J.-P. The Pigmentary System: Physiology and Pathophysiology. Blackwell Publishing Ltd, 2006.

Polubothu S, Kinsler VA. Final congenital melanocytic naevi colour is determined by normal skin colour and unaltered by superficial removal techniques: a longitudinal study. The British journal of dermatology 2019.

Polubothu S, McGuire N, Al-Olabi L, Baird W, Bulstrode N, Chalker J, et al. Does the gene matter? Genotype-phenotype and genotype-outcome associations in congenital melanocytic naevi. The British journal of dermatology 2019.

Ray KK, Wright RS, Kallend D, Koenig W, Leiter LA, Raal FJ, et al. Two Phase 3 Trials of Inclisiran in Patients with Elevated LDL Cholesterol. The New England journal of medicine 2020;382(16):1507-19.

Reshetnyak AV, Nelson B, Shi X, Boggon TJ, Pavlenco A, Mandel-Bausch EM, et al. Structural basis for KIT receptor tyrosine kinase inhibition by antibodies targeting the D4 membrane-proximal region. Proceedings of the National Academy of Sciences of the United States of America 2013;110(44):17832-7.

Salgado CM, Basu D, Nikiforova M, Bauer BS, Johnson D, Rundell V, et al. BRAF mutations are also associated with neurocutaneous melanocytosis and large/giant congenital melanocytic nevi. Pediatric and developmental pathology : the official journal of the Society for Pediatric Pathology and the Paediatric Pathology Society 2015;18(1):1-9.

Tagalakis AD, Lee DH, Bienemann AS, Zhou H, Munye MM, Saraiva L, et al. Multifunctional, self-assembling anionic peptide-lipid nanocomplexes for targeted siRNA delivery. Biomaterials 2014;35(29):8406-15.

Takahashi M, Hohjoh H. A novel measurement of allele discrimination for assessment of allele-specific silencing by RNA interference. Mol Biol Rep 2014;41(11):7115-20.

Tang J, Fewings E, Chang D, Zeng H, Liu S, Jorapur A, et al. The genomic landscapes of individual melanocytes from human skin. Nature 2020;586(7830):600-5.

Uhlen M, Fagerberg L, Hallstrom BM, Lindskog C, Oksvold P, Mardinoglu A, et al. Proteomics. Tissue-based map of the human proteome. Science 2015;347(6220):1260419.

van Laethem JL. Ki-ras oncogene mutations in chronic pancreatitis: which discriminating ability for malignant potential? Annals of the New York Academy of Sciences 1999;880:210-8.

Wheatley SP, Altieri DC. Survivin at a glance. J Cell Sci 2019;132(7).

Zhou Y, Zhou B, Pache L, Chang M, Khodabakhshi AH, Tanaseichuk O, et al. Metascape provides a biologist-oriented resource for the analysis of systems-level datasets. Nat Commun 2019;10(1):1523.

Figure Legends

Figure 1 Identification of siRNA with allelic discrimination for naevus cell causing *NRAS* variant. a, siRNA were designed with a "walking" approach over the variant of interest (*NRAS* c.181C>A; p.Q61K) (Vertical grey bar). Note that the sequences illustrated in the panel are the passenger strands for ease of interpreting corresponding nucleotides. siRNAs 1, 8 and 15 are colour coded for reference in other panels of this figure. **b,** The impact of siRNA treatment (48 hours) on *NRAS* transcript expression was investigated in HCT116 cells with qPCR. siRNA8 (blue) and siRNA15 (red) were selected based on their propensity to reduce expression of the *NRAS* variant and not WT *NRAS*. siRNA1 (green) was included in these experiments as a comparative control because it minimised both variant and WT *NRAS* expression. **c,** Assessment of allelic discrimination. Positive values indicate specificity for the *NRAS* variant, negative values indicate specificity for the *NRAS* WT mRNA transcript. **d,e,** RNA-seq confirms that the selected candidates do selectively minimise expression of the *NRAS* variant (**d**) compared to WT *NRAS* (**e**). **f,g,** Volcano plots demonstrating the impact of siRNA candidates on the transcriptome. Circles/arrows mark the position of *NRAS* in this data set. N = 3 replicates; bars = mean; error bars = SD, one-way ANOVA.

Figure 2 *siNRAS*^{Q61K} treatment decreases MAPK activation and reveals pathways/genes regulated by *NRAS*^{Q61K} expression in naevus cells. a, In vitro culture of patient-derived naevus cells without feeder cells. Naevus cells are positive for nuclear melanocyte marker SOX10 and cytoplasmic melanocyte marker tyrosinase. Scale bar = 100µm. **b,** Selective proliferation of patient-derived naevus cells reveal the somatic *NRAS* c.181C>A variant. **c,** Relative levels of *NRAS*^{Q61K} (*NRAS*$^{c.181C>A}$) mRNA following *siNRAS*^{Q61K} treatment normalised to untreated cells. **d,** Relative levels of *NRAS*^{WT} mRNA following *siNRAS*^{Q61K} treatment normalised to untreated cells. **e,** RNAseq normalised counts for *NRAS*. Fraction of *NRAS*^{WT} and *NRAS*^{Q61K} transcript were calculated based on reads covering the location of the *NRAS* variant. **f-h,** Relative levels of total NRAS protein (**f,g**) and MAPK activation (pERK) (**f,h**) following *siNRAS*^{Q61K} treatment normalised to untreated cells. **i,** Relative proliferation rate as assessed with EdU incorporation during final 24 hours of *siNRAS*^{Q61K} treatment (48 hours). **j,** Relative proliferation of naevus cells during 48 hour treatment (hours 24-48) using ptychographic imaging/analysis. **k,** Heatmap illustrating genes in pathways responding to *siNRAS*^{Q61K} (*Metascape WP2290 RALA downstream regulated genes; M53 PID INTEGRIN3

PATHWAY; GO0007346 regulation of mitotic cell cycle; GO:0007272 ensheathment of neurons; GO:0008366 axon ensheathment) and melanocyte stem cell and differentiation associated genes which were relatively unaffected. **l,** Volcano plot illustrating fold change and false discovery rate. Genes with very strong significance and fold change are labelled. N = 4 patients (**c,d,g,h**), N = 7 patients (**e,i,k,l**), bars = mean; error bars = SD, one-tailed unpaired t-test. N = 4 patients; points = mean; error bars = SD, one-way ANOVA (**j**).

Figure 3 Treatment of naevus cells with *siNRAS^{Q61K}* leads to endoplasmic reticulum (ER) stress and apoptosis. a, ER localised expression of ARL6IP1 in patient-derived naevus cells. Scale bar = 50µm. **b-e,** Following 48 hours of treatment with *siNRAS^{Q61K}* the expression of *ARL6IP1* mRNA is decreased (**b**), the expression of ARL6IP1 protein is decreased (**c**), the expression of ER stress sensor, *ERN1 (IRE1)* is increased (**d**), and the expression of anti-apoptotic *Survivin (BIRC5)* is decreased (**e**). **f,** Caspase 3/7 activity in cells treated with *siNRAS^{Q61K}* over 7 days. N = 7 patients (**b,d,e**), N = 8 patients (**c**), bars = mean, error bars = SD, one-tailed unpaired t-test. N = 4, bars = mean, error bars = SD, two-way ANOVA (**f**).

Figure 4 Treatment of naevus cells with *siNRAS^{Q61K}* permits effectiveness and synergy with trametinib. a,b, Relative proliferation rate as assessed with EdU incorporation during final 24 hours of combined *siNRAS^{Q61K}* and trametinib treatment (5nM and 12.5nM) (48 hours). Scale bar = 200µm. **c,** Caspase 3/7 activity in patient naevus cells after 5 days of treatment with *siNRAS^{Q61K}* in combination with trametinib (5nM and 12.5nM). **d,** Caspase 3/7 activity in cells treated with (perforated line) or without (solid line) 12.5nM trametinib in combination with *siNRAS^{Q61K}* over 5 days. N = 4 patients, bars = mean, error bars = SD, one-way ANOVA (**a,c**). N = 5 technical replicates for each patient, points = mean, error bars = SD, one-way ANOVA (**d**).

Figure 5 *In vivo* delivery and knockdown of naevus cell causing *NRAS* variant with *siNRAS^{Q61K}* loaded lipid nanoparticles. a, Intradermal injection of naevus patient biopsy with siRNA-cy5 encapsulated in lipid nanoparticles. Scale bar = 100µm. **b,** siRNA encapsulated in lipid nanoparticles could be delivered to the cells of the dermis of naevus patient biopsy. **c,** siRNA not encapsulated in lipid nanoparticles delivered relatively little into the cells of the dermis of naevus patient biopsy. **d,** Naevus causing *NRAS* variant expression driven by the melanocyte specific tyrosinase promoter causes ectopic pigment cells in the dermis and hypodermis of *Tyr::NRAS^{Q61K}* mice. Scale bar = 200µm. **e,** No ectopic pigment cells in the dermis or hypodermis of *NRAS^{WT}* mice. Scale bar = 200µm. **f,** Intradermal injection of *Tyr::NRAS^{Q61K}* mice with *siNRAS^{Q61K}* decreased the expression of naevus cell causing *NRAS* variant. **g,** Intradermal injection of *Tyr::NRAS^{Q61K}* mice with *siNRAS^{Q61K}* did not decrease the expression of endogenous mouse *Nras^{WT}*. N = 8, data pooled together from two experiments, points = individual mice (closed circles = mice treated for 24 hours, open circles = mice treated for 48 hours), bars = mean, error bars = SD, unpaired one-tailed t-test (**f,g**).

a

5'-3' siRNA Sequence

siRNA1	AUACUGGAUACAGCUGGAATT
siRNA2	UACUGGAUACAGCUGGAATT
siRNA3	ACUGGAUACAGCUGGAAATT
siRNA4	CUGGAUACAGCUGGAAAGTT
siRNA5	UGGAUACAGCUGGAAAGATT
siRNA6	GGAUACAGCUGGAAAGAATT
siRNA7	GAUACAGCUGGAAAGAAGTT
siRNA8	AUACAGCUGGAAAGAAGATT
siRNA9	UACAGCUGGAAAGAAGAGTT
siRNA10	ACAGCUGGAAAGAAGAGUTT
siRNA11	CAGCUGGAAAGAAGAGUATT
siRNA12	AGCUGGAAAGAAGAGUACTT
siRNA13	GCUGGAAAGAAGAGUACATT
siRNA14	CUGGAAAGAAGAGUACAGTT
siRNA15	UGGAAAGAAGAGUACAGUTT
siRNA16	GGAAAGAAGAGUACAGUGTT
siRNA17	GAAAGAAGAGUACAGUGCTT
siRNA18	AAAGAAGAGUACAGUGCCTT
siRNA19	AAAGAAGAGUACAGUGCCATT

5'-3' Genomic Sequence (corresponds to *NRAS* c.162-202)

$NRAS^{WT}$	CATACTGGATACAGCTGGACAAGAAGAGTACAGTGCCATG
$NRAS^{Q61K}$	CATACTGGATACAGCTGGAAAAGAAGAGTACAGTGCCATG

b

	$NRAS^{Q61K}$ Cells		$NRAS^{WT}$ Cells	
	Change	*p-value*	Change	*p-value*
siRNA1*	-0.8794	0.0161	-0.8630	0.0031
siRNA2	-0.8520	0.0163	-0.8503	0.0040
siRNA3	-0.8500	0.0034	-0.8314	0.0066
siRNA4	-0.6667	0.0764	-0.6409	0.0008
siRNA5	-0.8296	0.0137	-0.8133	0.0014
siRNA6	-0.9082	0.0151	-0.8540	0.0014
siRNA7	-0.7913	0.0334	-0.8003	<0.0001
siRNA8†	-0.7515	0.0261	-0.2330	0.0550
siRNA9	-0.6981	0.0584	-0.6255	0.0042
siRNA10	-0.8557	0.0496	-0.4155	0.0443
siRNA11	-0.8268	0.0493	-0.6397	0.0015
siRNA12	-0.7772	0.0686	-0.0083	0.4658
siRNA13	-0.8496	0.0050	-0.6213	0.0048
siRNA14	-0.7074	0.0216	-0.5541	0.0993
siRNA15†	-0.5639	0.0135	-0.0222	0.3641
siRNA16	-0.5511	0.1173	-0.5671	0.0261
siRNA17	-0.1227	0.2826	-0.6107	0.0059
siRNA18	-0.6083	0.0038	-0.6573	0.0457
siRNA19	-0.5904	0.0122	-0.7928	0.0040

*Candidate selected for low allelic discrimination

†Candidates selected for best allelic discrimination

c

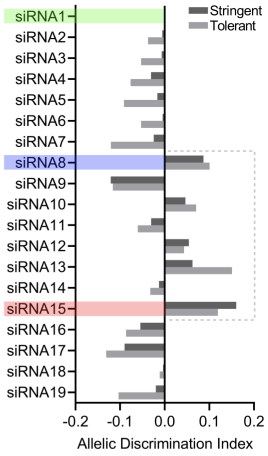

d

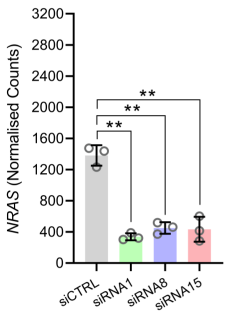

e

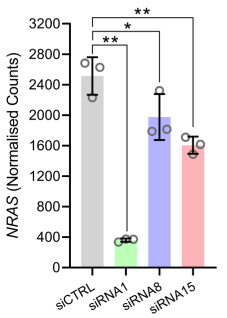

f

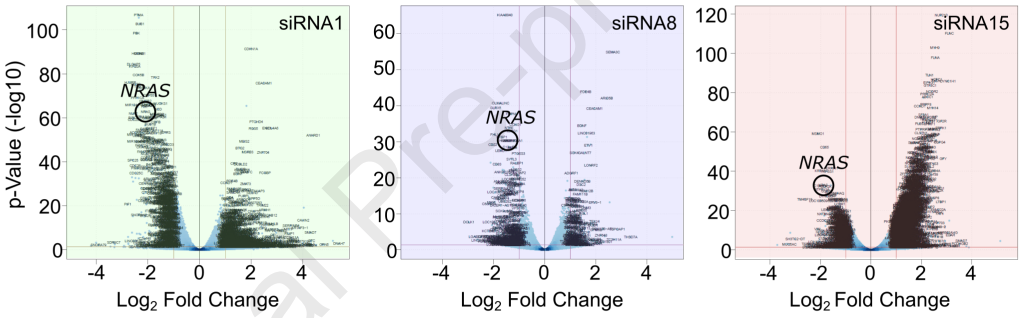

g

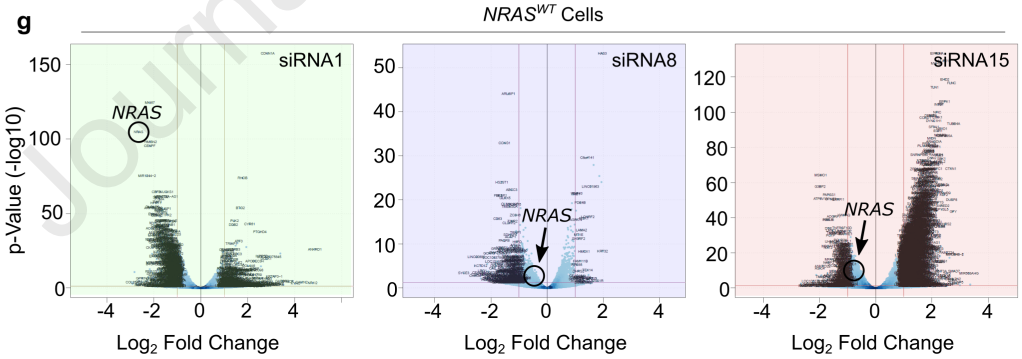

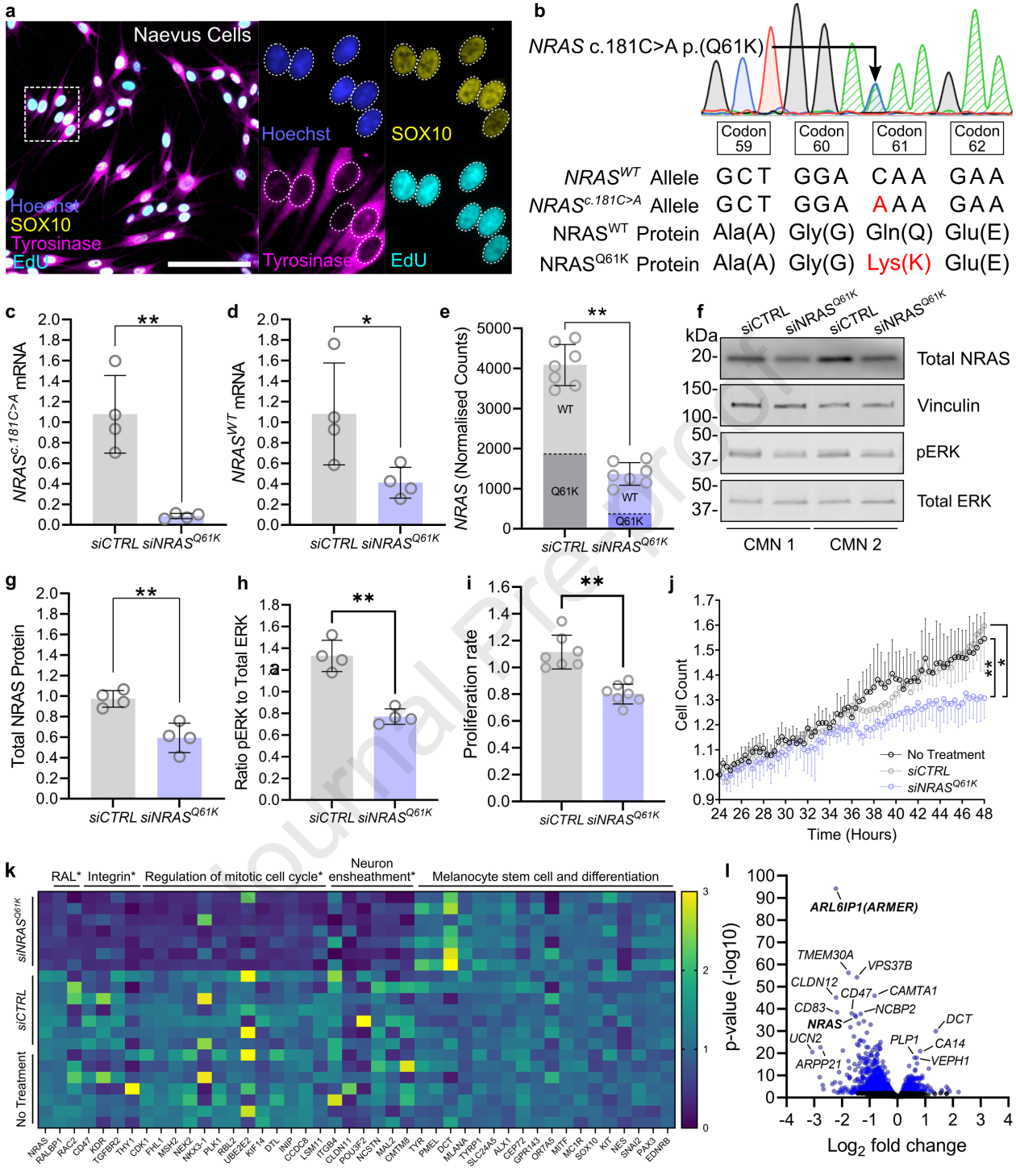

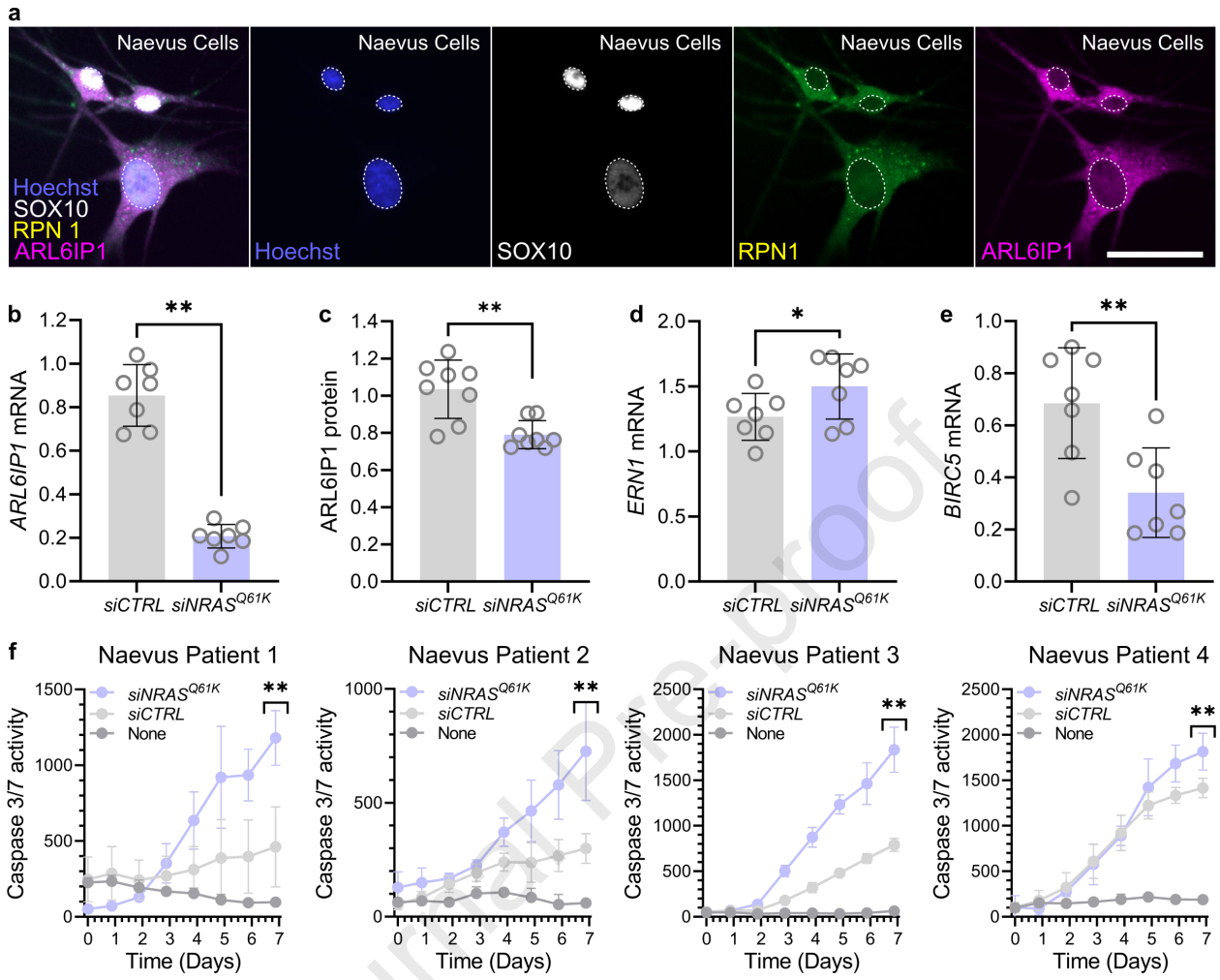

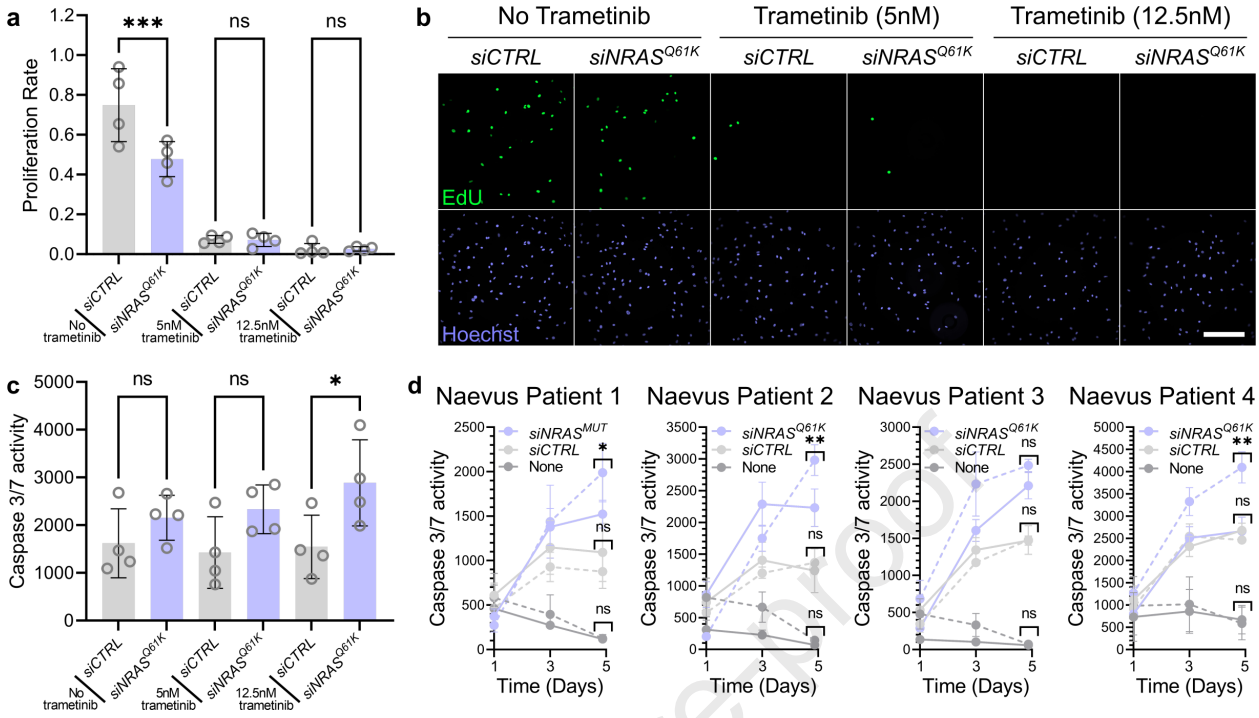

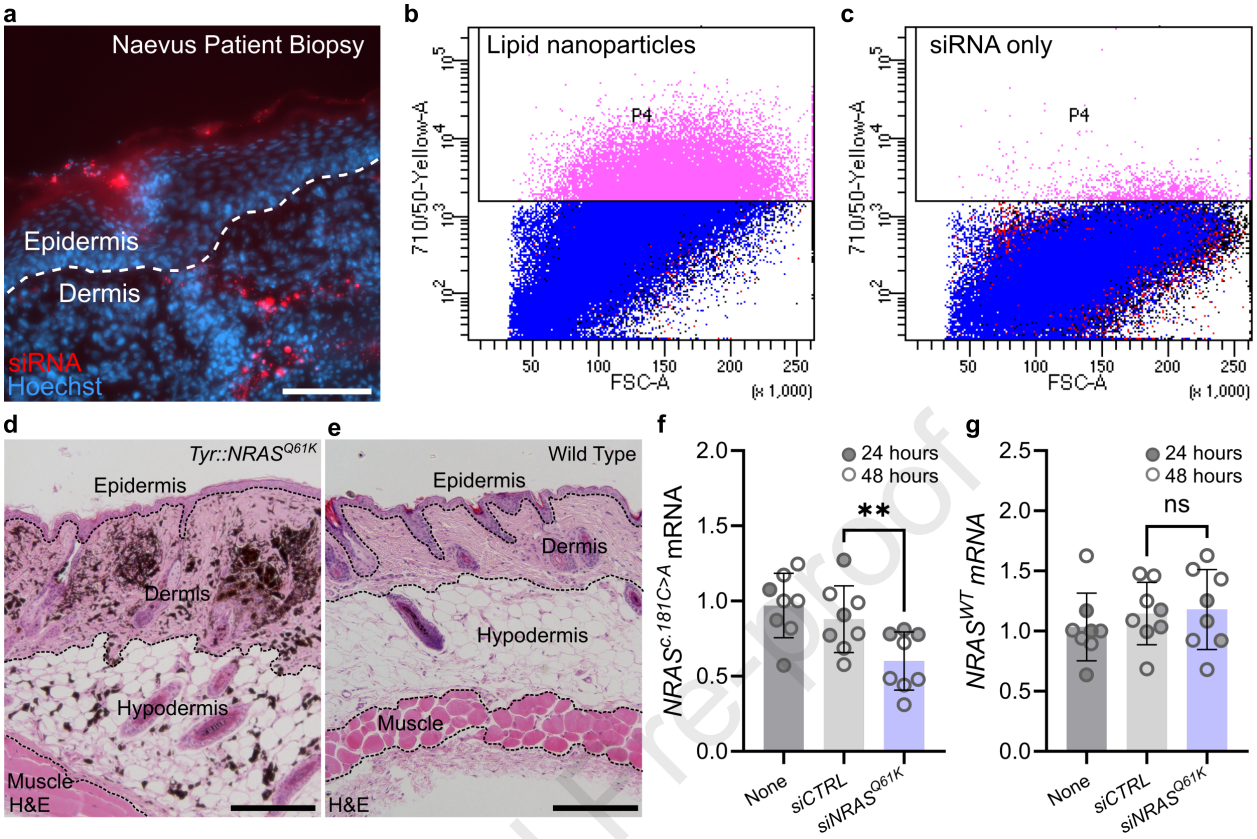

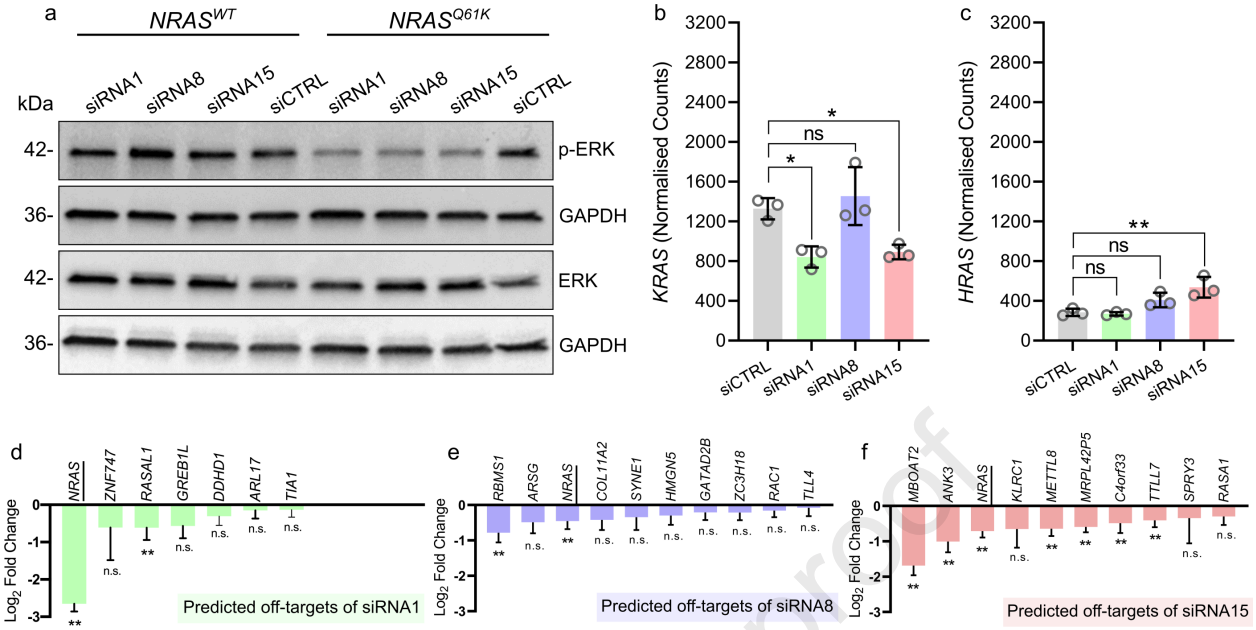

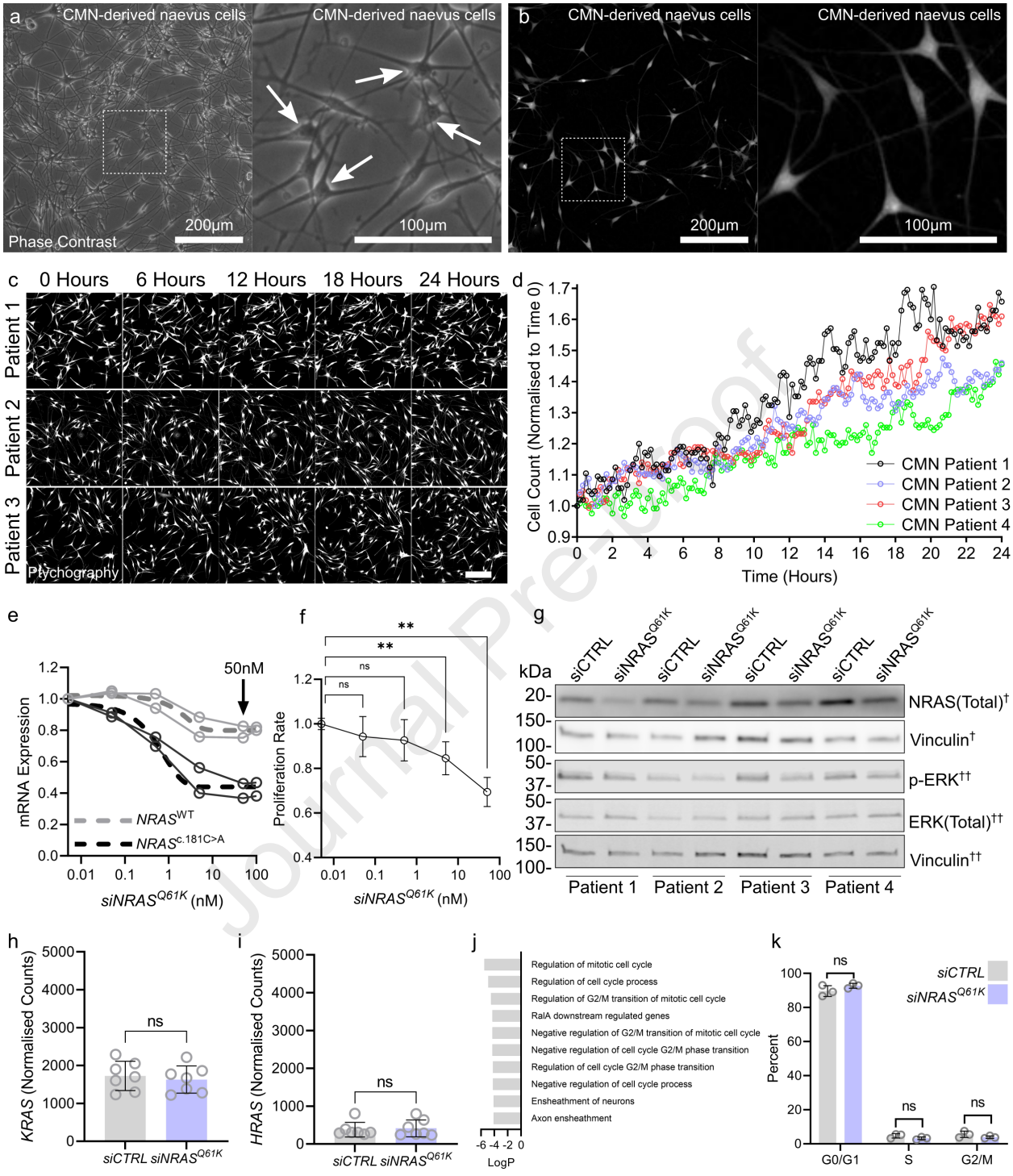

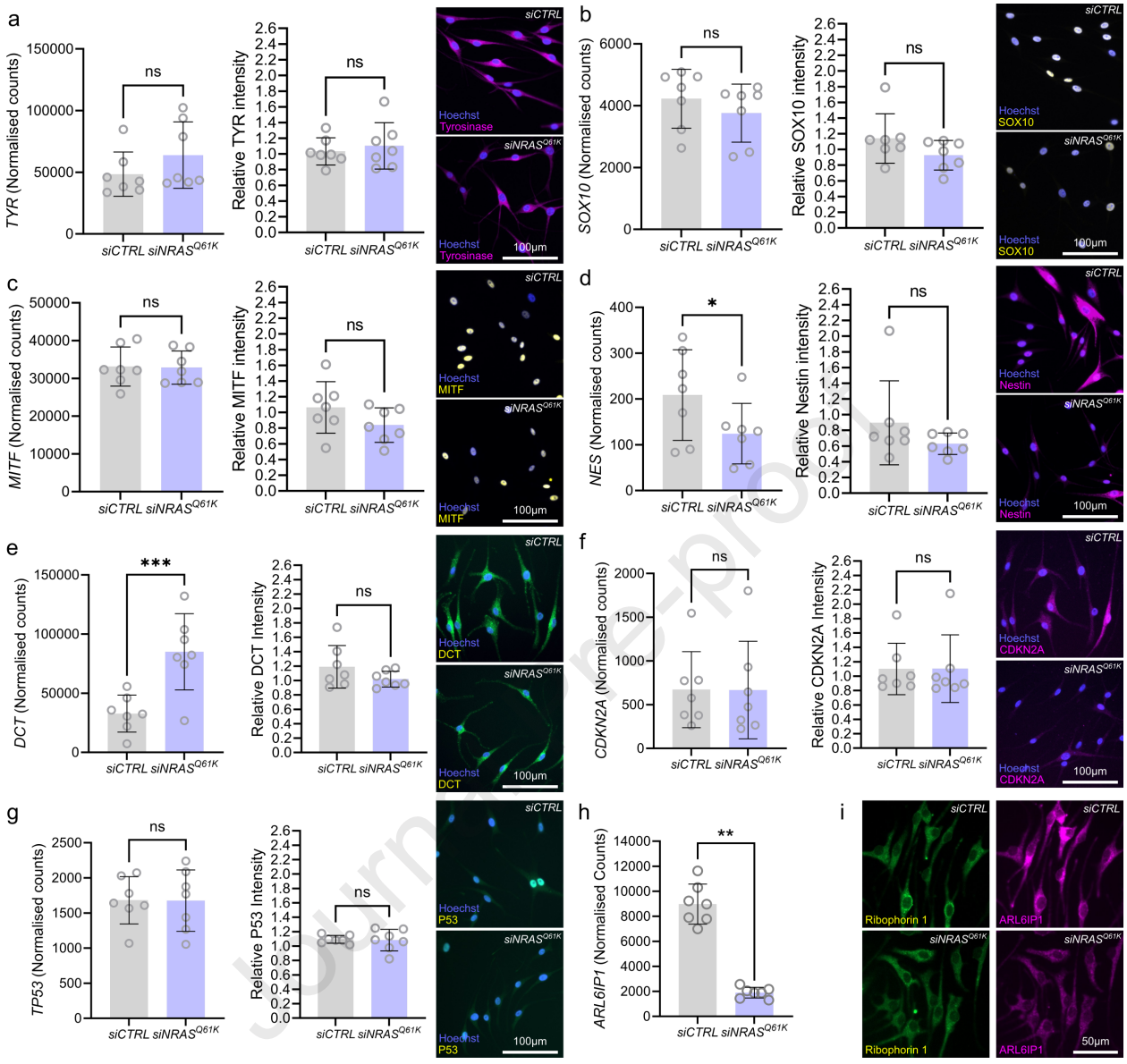
a
TYR (Normalised counts)
ns
siCTRL siNRASQ61K
Relative TYR intensity
ns
siCTRL siNRASQ61K
siCTRL
Hoechst Tyrosinase
siNRASQ61K
Hoechst Tyrosinase
100µm
b
SOX10 (Normalised counts)
ns
siCTRL siNRASQ61K
Relative SOX10 intensity
ns
siCTRL siNRASQ61K
siCTRL
Hoechst SOX10
siNRASQ61K
Hoechst SOX10
100µm
c
MITF (Normalised counts)
ns
siCTRL siNRASQ61K
Relative MITF intensity
ns
siCTRL siNRASQ61K
siCTRL
Hoechst MITF
siNRASQ61K
Hoechst MITF
100µm
d
NES (Normalised counts)
*
siCTRL siNRASQ61K
Relative Nestin intensity
ns
siCTRL siNRASQ61K
siCTRL
Hoechst Nestin
siNRASQ61K
Hoechst Nestin
100µm
e
DCT (Normalised counts)
***
siCTRL siNRASQ61K
Relative DCT Intensity
ns
siCTRL siNRASQ61K
siCTRL
Hoechst DCT
siNRASQ61K
Hoechst DCT
100µm
f
CDKN2A (Normalised counts)
ns
siCTRL siNRASQ61K
Relative CDKN2A Intensity
ns
siCTRL siNRASQ61K
siCTRL
Hoechst CDKN2A
siNRASQ61K
Hoechst CDKN2A
100µm
g
TP53 (Normalised counts)
ns
siCTRL siNRASQ61K
Relative P53 Intensity
ns
siCTRL siNRASQ61K
siCTRL
Hoechst P53
siNRASQ61K
Hoechst P53
100µm
h
ARL6IP1 (Normalised Counts)
**
siCTRL siNRASQ61K
i
siCTRL
Ribophorin 1
siCTRL
ARL6IP1
siNRASQ61K
Ribophorin 1
siNRASQ61K
ARL6IP1
50µm

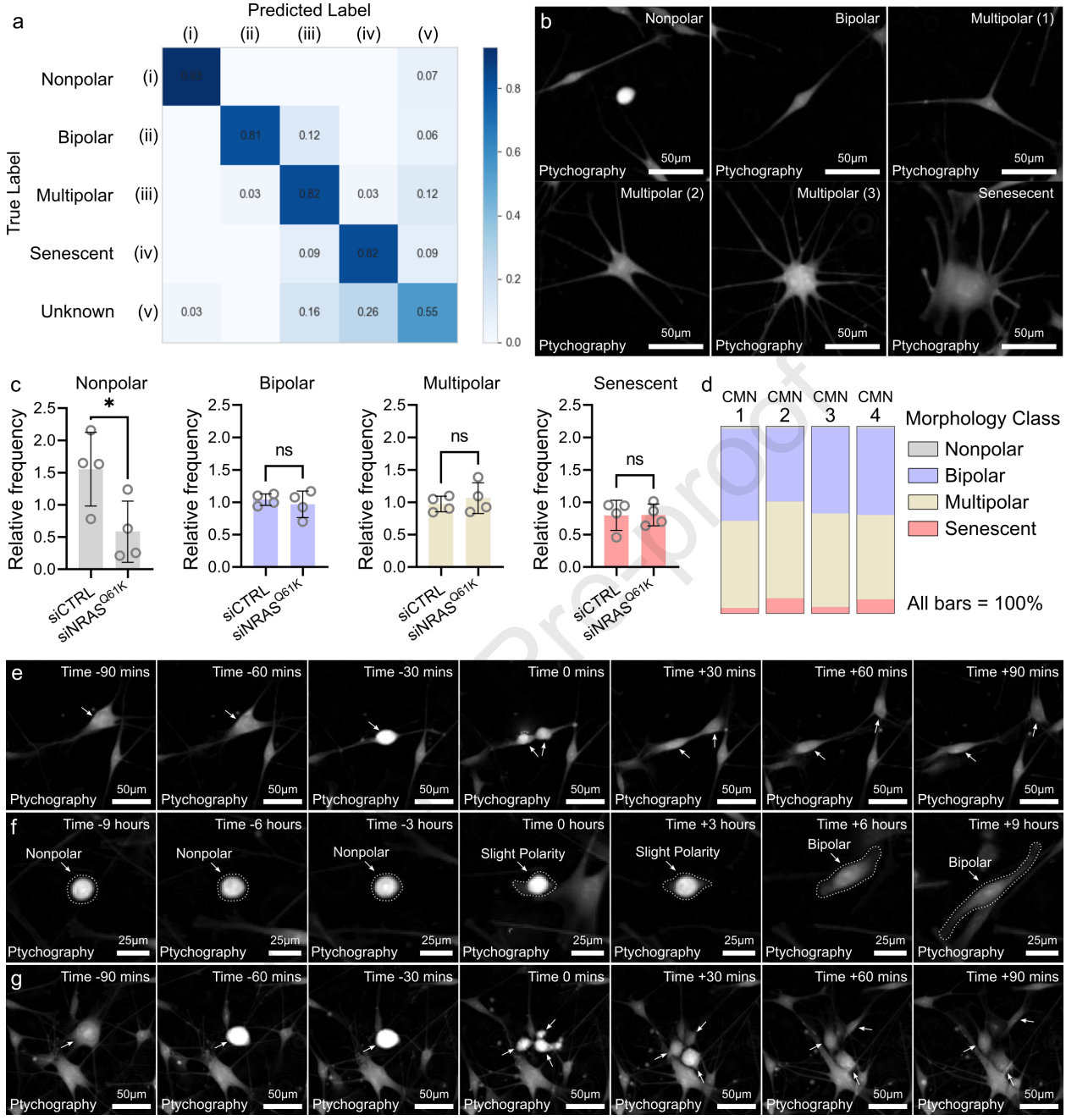
a
Predicted Label
(i)
(ii)
(iii)
(iv)
(v)
True Label
Nonpolar
Bipolar
Multipolar
Senescent
Unknown
0.93
0.07
0.81
0.12
0.06
0.03
0.82
0.03
0.12
0.09
0.82
0.09
0.03
0.16
0.26
0.55
0.8
0.6
0.4
0.2
0.0
b
Nonpolar
Bipolar
Multipolar (1)
Multipolar (2)
Multipolar (3)
Senescent
Ptychography
50μm
c
Nonpolar
Bipolar
Multipolar
Senescent
Relative frequency
2.5
2.0
1.5
1.0
0.5
0.0
*
ns
siCTRL
siNRASQ61K
d
CMN 1
CMN 2
CMN 3
CMN 4
Morphology Class
Nonpolar
Bipolar
Multipolar
Senescent
All bars = 100%
e
Time -90 mins
Time -60 mins
Time -30 mins
Time 0 mins
Time +30 mins
Time +60 mins
Time +90 mins
Ptychography
50μm
f
Time -9 hours
Time -6 hours
Time -3 hours
Time 0 hours
Time +3 hours
Time +6 hours
Time +9 hours
Nonpolar
Slight Polarity
Bipolar
25μm
g
Time -90 mins
Time -60 mins
Time -30 mins
Time 0 mins
Time +30 mins
Time +60 mins
Time +90 mins
50μm

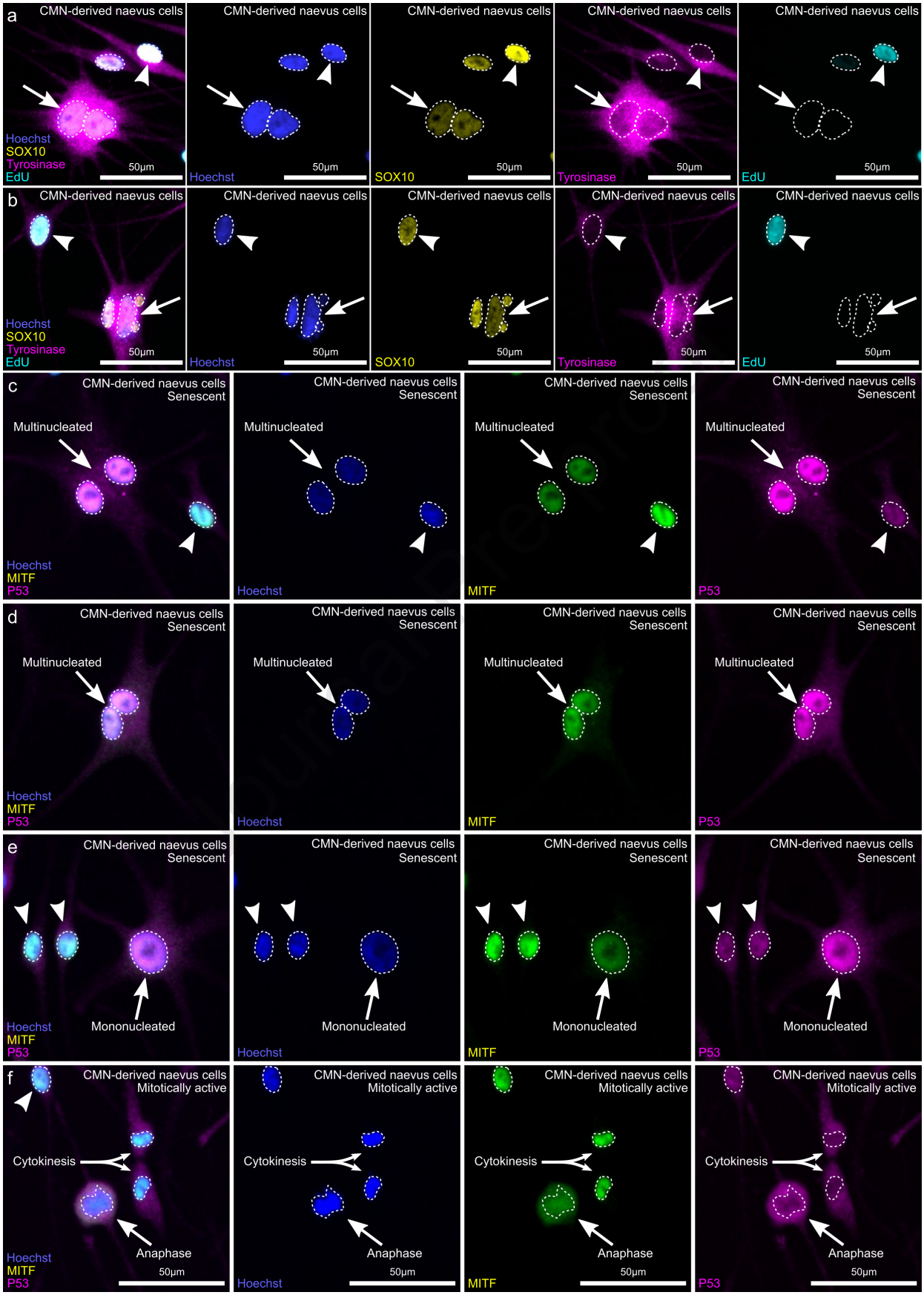
a
CMN-derived naevus cells
Hoechst
SOX10
Tyrosinase
EdU
50μm
Hoechst
SOX10
Tyrosinase
EdU
b
c
Senescent
Multinucleated
MITF
P53
d
e
Mononucleated
f
Mitotically active
Cytokinesis
Anaphase

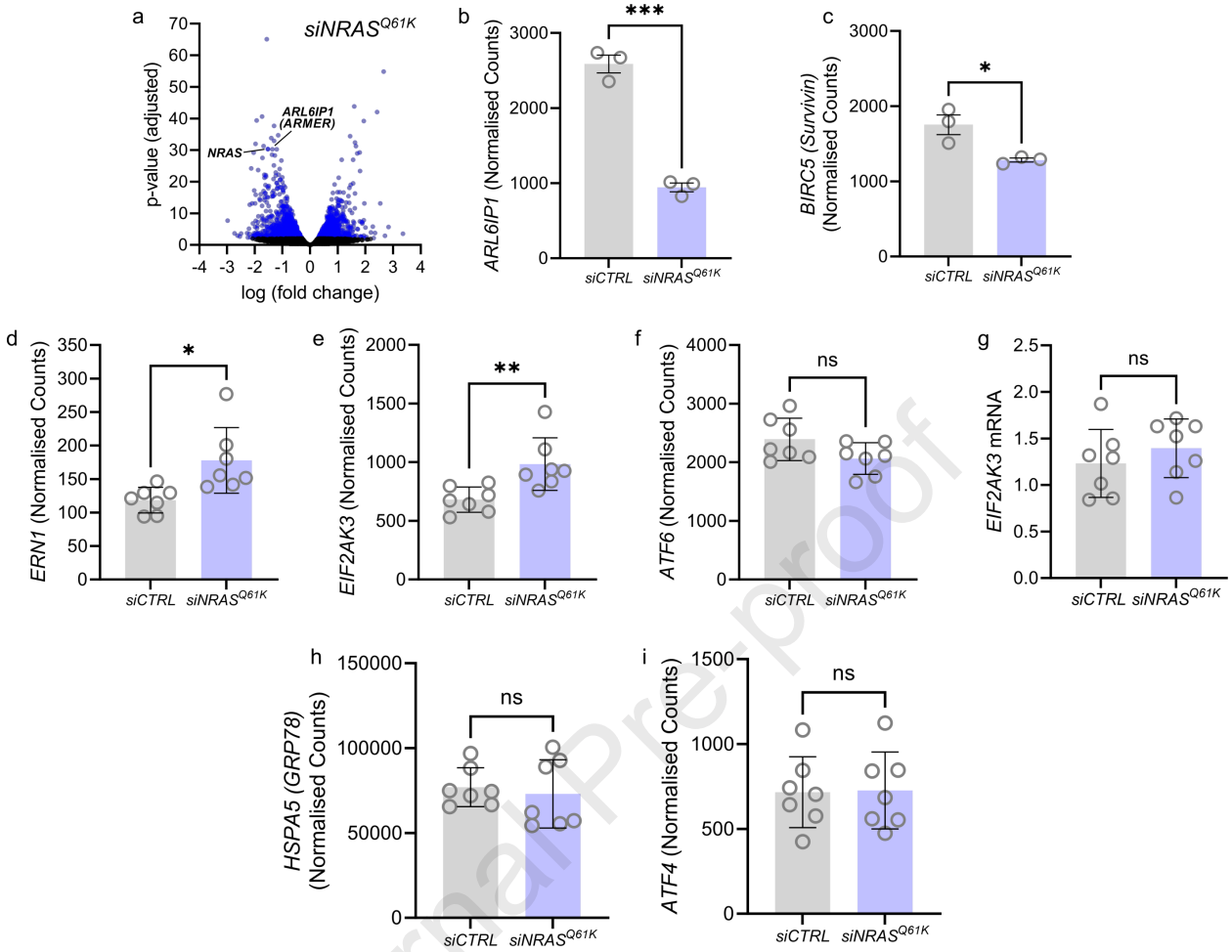

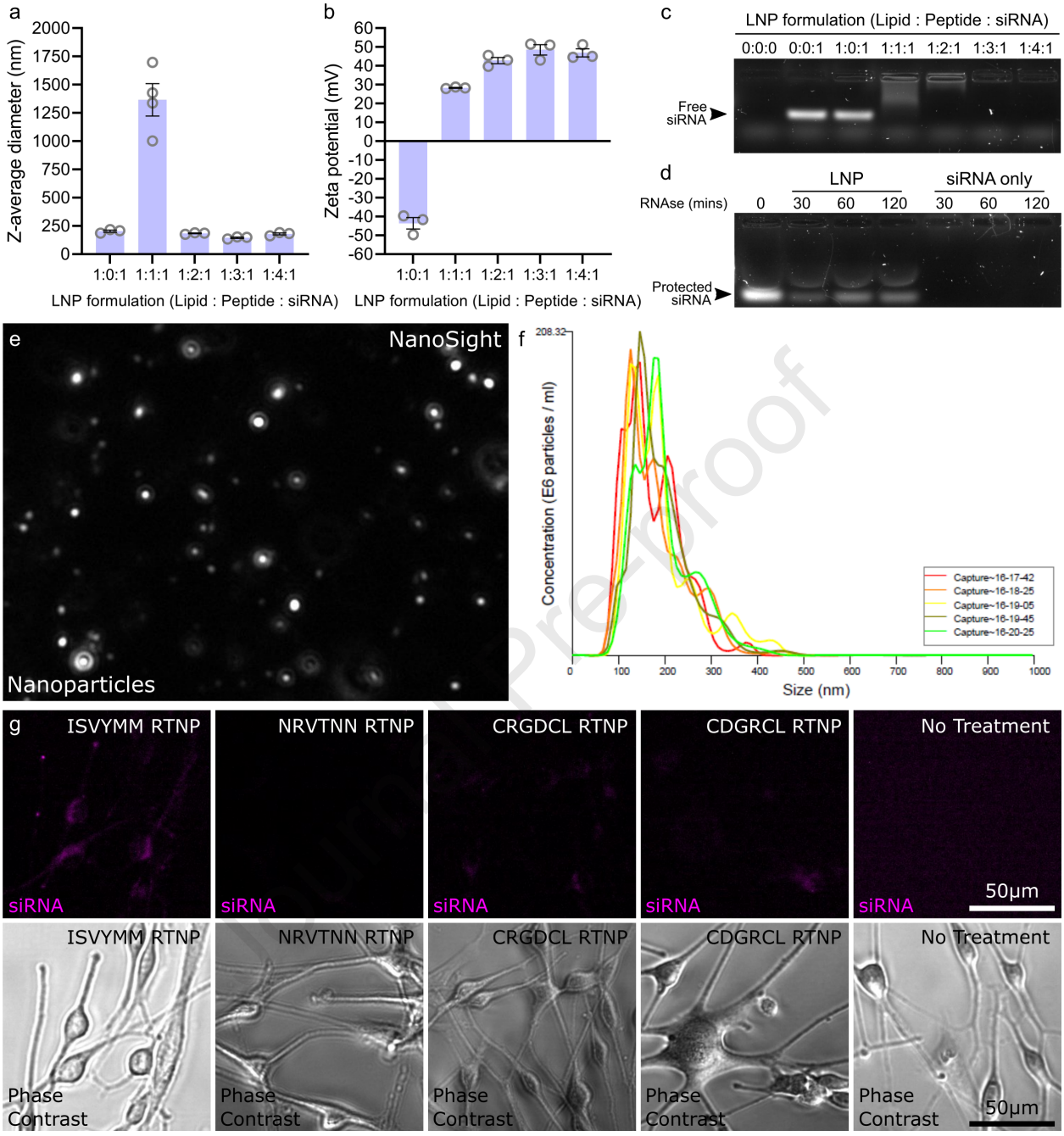
a
Z-average diameter (nm)
2000
1750
1500
1250
1000
750
500
250
0
1:0:1 1:1:1 1:2:1 1:3:1 1:4:1
LNP formulation (Lipid : Peptide : siRNA)
b
Zeta potential (mV)
60
50
40
30
20
10
0
-10
-20
-30
-40
-50
-60
1:0:1 1:1:1 1:2:1 1:3:1 1:4:1
LNP formulation (Lipid : Peptide : siRNA)
c
LNP formulation (Lipid : Peptide : siRNA)
0:0:0 0:0:1 1:0:1 1:1:1 1:2:1 1:3:1 1:4:1
Free siRNA
d
LNP
siRNA only
RNAse (mins)
0 30 60 120 30 60 120
Protected siRNA
e
NanoSight
Nanoparticles
f
208.32
Concentration (E6 particles / ml)
Capture~16-17-42
Capture~16-18-25
Capture~16-19-05
Capture~16-19-45
Capture~16-20-25
0 100 200 300 400 500 600 700 800 900 1000
Size (nm)
g
ISVYMM RTNP
NRVTNN RTNP
CRGDCL RTNP
CDGRCL RTNP
No Treatment
siRNA
50μm
Phase Contrast

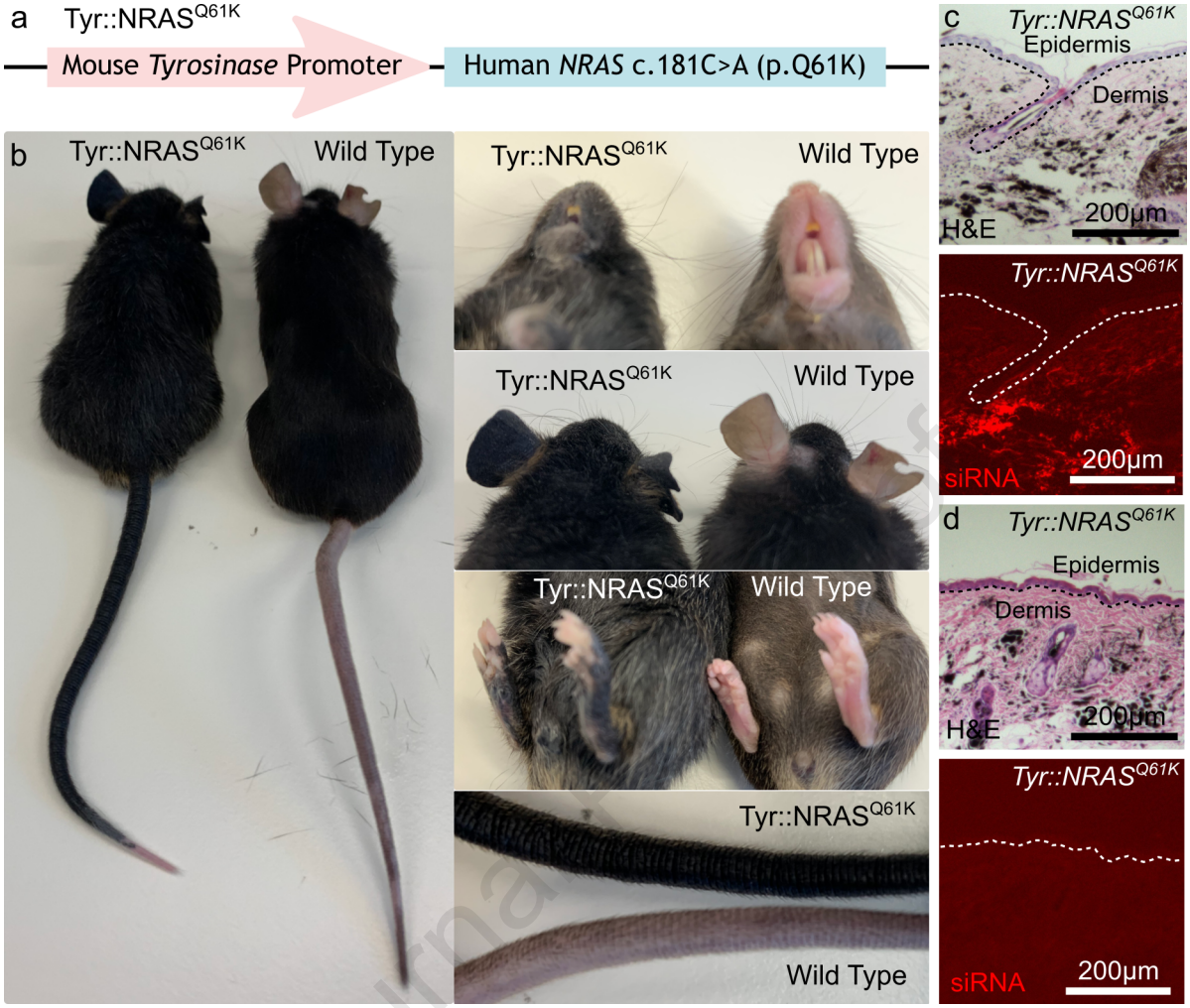

Supplementary Text

Title

RNA therapy for oncogenic *NRAS*-driven naevi induces apoptosis

Authors

Dale Bryant[1,2], Sara Barberan-Martin[1,2], Ruhina Maeshima[2], Ignacio del Valle Torres[1,2], Mohammad Rabii[1,2], William Baird[2], Aimie Sauvadet[1,2], Charalambos Demetriou[2], Phoebe Jones[1,2], Nicole Knöpfel[1,2,3], Fanourios Michailidis[1,2], Melissa Riachi[1,2], Dorothy C Bennett[4], Davide Zecchin[1,2], Alan Pittman[4], Satyamaanasa Polubothu[1,2,3], Stephen Hart[2], Veronica A. Kinsler[1,2,3]

Affiliations

1. Mosaicism and Precision Medicine Lab, The Francis Crick Institute, London, UK
2. Genetics and Genomic Medicine, UCL GOS Institute of Child Health, London, UK
3. Paediatric Dermatology, Great Ormond Street Hospital for Children, London, UK
4. St George's University of London, London, UK

Corresponding author

Veronica Kinsler, Mosaicism and Precision Medicine Laboratory, The Francis Crick Institute, London, UK; 020 3796 0000; v.kinsler@ucl.ac.uk

Key Words: siRNA, nanoparticle, oncogene, skin, melanocyte

Conflict of interest statement

The authors have declared that no conflict of interest exists. Patent application number GB2216028.7 has been filed in relation to this work on behalf of DB and VK.

Supplementary Figure 1 Impact of siRNA candidates on MAPK activation and *NRAS* homologues in HCT116 cells. a, siRNA candidates decrease p-ERK in the *NRAS* variant cell line (c.181C>A, $NRAS^{Q61K}$) compared to the *NRAS* wild type cell line (c.181C, $NRAS^{WT}$). Total ERK and GAPDH are included as comparative loading controls. **b,c,** Impact 48 hour siRNA candidate treatment on homologues **b,** *KRAS* and **c,** *HRAS* in HCT116 cells (c.181C, $NRAS^{WT}$). **d-f,** Impact of siRNA candidates on genes containing sequences with similarity to the target sequence of **d,** siRNA1, **e,** siRNA8 and **f,** siRNA15. (*$p \leq 0.05$, **$p \leq 0.1$, n=3, bars = mean, error bars = SEM, ANOVA)

Supplementary Figure 2 Targeting *NRAS* variant in naevus cells from CMN patient tissue. a, Naevus cells cultured in feeder-free conditions imaged with phase contrast. Scale bar = 200µm. **b,** Ptychographic processing of phase contrast data provides high contrast images that lend themselves to segmentation. Scale bar = 200µm. **c,** Ptychographic images of patient cell lines over 24 hours. Scale bar = 200µm. **d,** Cell counts using ptychographic images of patient cell lines over 24 hours normalised to time 0, demonstrating a degree of inter-patient variability in growth rate as expected from primary cultures. **e,** Dose-dependent effects on $NRAS^{WT}$ (grey) and $NRAS^{c.181C>A}$ (black) transcript expression following 48 hours of treatment of naevus cells with different concentrations of siRNA8 ($siNRAS^{Q61K}$). RNAiMAX was used as the delivery vector and the arrow is the concentration suggested in the manufacturers protocol. Two patient derived naevus cell lines were tested (individual circles at each time point), with the perforated line representing the mean of the two. **f,** Dose-dependent effects of $siNRAS^{Q61K}$ treatment on proliferation (48 hours). **g,** Western blot of protein lysates collected from all naevus patient cell cultures treated with *siCTRL* or $siNRAS^{Q61K}$ for 48 hours. All images are from the same blot. †Chemiluminescence imaging was required to detect NRAS protein levels as it was more sensitive than the Odyssey. ††The Odysee (fluorescence) was required to assess pERK levels as it permitted simultaneous measurement of total ERK and pERK by using secondary antibodies conjugated to fluorophores of different wavelengths. **h,i,** impact of 48 hour $siNRAS^{Q61K}$ treatment of naevus cells on *NRAS* homologues *KRAS* (**h**) and *HRAS* (**i**). **j,** Top 10 enriched pathways from genes with expression changed (criteria: >1fold; <-1fold; p≤0.05) by 48 hours $siNRAS^{Q61K}$ treatment of naevus cells. **k,** fraction of naevus cells in each stage of the cell cycle (estimated based on DNA content) following 48 hours $siNRAS^{Q61K}$ treatment.

Supplementary Figure 3 Gene expression and antibody reactivity to naevus cells (*NRAS c.181C>A (p.Q61K)* treated with $siNRAS^{Q61K}$ for 48 hours. RNAseq data (normalised counts) and relative signal intensity from antibody reactivity for **a,** TYR, **b,** SOX10, **c,** MITF, **d,** NES, **e,** DCT, **f,** CDKN2A, **g,** P53 and **h,** *ARL6IP1* (note quantification of ARL6IP1 antibody reactivity is in main text). *N*=7 (Individual values), bars = mean, error bars = SD, paired t-test. **i,** Immunocytochemistry showing decreased ARL6IP1 (magenta) expression in response to 48 hour $siNRAS^{Q61K}$ treatment. ARL6IP1 was assessed alongside an antibody targeting Ribophorin 1 (endoplasmic reticulum, green). **a-g** Scale bar = 200µm, **i** Scale bar = 50µm.

Supplementary Figure 4 Classification of naevus cell morphologies. a, Evaluation of classification tool presented as a confusion matrix. **b,** Increasing multipolar naevus cell morphologies (Multipolar 1-3) were considered as a single category in the analysis to improve accuracy of the classification tool. Scale bar = 50µm. **c,** Treatment of naevus cells with $siNRAS^{Q61K}$ (48 hours) decreases nonpolar cells. *N*=4; bars = mean; error bars = SD, one-tailed paired t-test. **d,** Comparable fractions of each cell morphology for four different CMN patient

cell lines. **e,** Ptychographic images over three hours during which a cell divides (time 0). Scale bar = 50µm. **f,** Ptychographic images over 18 hours during which a perpetual (at least nine hours) nonpolar naevus cell becomes polar (time 0). Scale bar = 25µm. **g,** Ptychographic images over three hours during which a single cell becomes three daughter cells (time 0). Scale bar = 50µm.

Supplementary Figure 5 Senescence in large and multinucleated naevus cells. Naevus cells (*NRAS c.181C>A (p.Q61K)*) with multiple nuclei containing **a,** two nuclei or **b,** fragmented nuclear compartments. **c-e,** naevus cells with multiple nuclei have elevated P53 expression (arrows). Cells with single nuclei are marked with arrow heads. **f,** Cells with morphologies/Hoechst staining indicative of anaphase and cytokinesis have low P53 expression. Scale bars = 50µm.

Supplementary Figure 6 Genes of interest in HCT116 dataset and endoplasmic reticulum stress associated genes in naevus cell RNAseq dataset. a-c, RNAseq expression data following 48 hour treatment of HCT116 cells (c.181C>A, NRASQ61K) with *siNRAS^{Q61K}*. **a,** Volcano plot showing comparable decrease of *ARL6IP1 (ARMER, apoptotic regulator in the membrane of the endoplasmic reticulum)* and *NRAS* expression. **b,** Decrease of *ARL6IP1* expression following treatment with *siNRAS^{Q61K}*. **c,** Decrease of *Survivin (BIRC5)* expression following treatment with *siNRAS^{Q61K}*. **d-f,** RNAseq expression data of the three primary ER stress regulators *ERN1 (IRE1)* (**d**), *EIF2AK3 (PERK)* (**e**) *ATF6* (**f**), HSPA5 (**h**) and ATF4 (**i**) after 48 hour treatment of naevus cells with *siNRAS^{Q61K}*. **g,** qPCR validation of *EIF2AK3* result on RNAseq did not return a statistically significant difference (**g**). *N*=7, bars = mean, error bars = SD, two-tailed upaired t-test.

Supplementary Figure 7 Lipid nanoparticles. The **a,** size (Zeta-average diameter), **b,** charge (Zeta-potential) and **c,** siRNA encapsulation of lipid nanoparticles formulated at different ratios were assessed. **d,** Formulation of lipid nanoparticles at 1:4:1 (lipid:peptide:siRNA) ratios protected siRNA from RNases better than siRNA alone. **e,** Visualisation and **f,** particle size distribution of RTNPs calculated with NanoSight instrument (Malvern). **g,** Delivery of siRNA-cy5 to naevus cells with RTNPs formulated using different peptides (KKKKKKKKKKKKKKKKGACXXXXXXCG) with the targeting motif (XXXXXX): ISVYMM (reported to bind to KIT), NRVTNN (predicted to bind to KIT), CRGDCL (reported to bind to α5β1, αvβ5, and αvβ3 integrin) and CDGRCL (no known target). Scale bar = 50µm.

Supplementary Figure 8 Intradermal delivery of *siRNA* in mouse model of CMN. a, Tyr::NRASQ61K mice (Tg(Tyr-NRAS*Q61K)1Bee in which expression of the human disease causing variant *NRAS c.181C>A,p.(Q61K)* is driven by the endogenous mouse tyrosinase promoter. **b,** Mice heterozygous for the transgene show widespread skin hyperpigmentation with accumulation of melanin producing cells within the dermis, recapitulating the human phenotype of CMN to a large degree. **c,d,** Biopsies of skin taken one hour after a single intradermal injection of **c,** a fluorescent siRNA-Cy5 within lipid nanoparticles or **d,** lipid nanoparticles only.

Supplementary Table 1 Formulation of naevus cell media.

Reagent	Vendor	Code	Formulation
Ham F-10 nutrient mix	ThermoFisher	11550043	Basal medium
Fibroblasts growth factor basic (bFGF)	PeproTech	100-18B	2.5 ng/ml
Endothelin-1 (ET-1)	Bachem	H-6995	10 ng/ml
3-isobutyl-1-methylxanthine (IBMX)	Sigma	I5879	31.5 µM
Cholera Toxin	Sigma	C8052	0.33 nM
Phorbol 12-myristate 13-acetate (TPA)	Sigma	P8139	5 nM
L-Glutamine	ThermoFisher	25030024	1x
Foetal bovine serum	Gibco	10270106	5% of total volume
Stem cell factor (SCF)	Peprotech	300-07	20 ng/ml
Penicillin-Streptomycin	Gibco	15070063	1x
Amphotericin B	Sigma	A2942	1x

Supplementary Table 2 Antibodies used for immunocytochemistry.

Target	Species	Type	Code	Dilution	Blocking
Tyrosinase	Rabbit	IgG	AB170905	1:100	PBS, 10%FBS, 0.01% Triton X-100
MITF	Mouse	IgG1	AB3201	1:100	PBS, 10%FBS, 0.01% Triton X-100
Nestin	Rabbit	IgG	AB105389	1:100	PBS, 10%FBS, 0.01% Triton X-100
SOX10	Mouse	IgG	SC-365692	1:100	PBS, 10%FBS, 0.01% Triton X-100
DCT	Rabbit	IgG	AB74073	1:200	PBS, 10%FBS, 0.01% Triton X-100
CDKN2A	Mouse	IgG2a	SC-56330	1:200	PBS, 10%FBS, 0.01% Triton X-100
P53	Rabbit	IgG	CST-9282	1:100	PBS, 10%FBS, 0.01% Triton X-100
ARL6IP1	Rabbit	IgG	GTX85516	1:500	PBS, 10%FBS, 0.01% Triton X-100
RPN1	Goat	IgG	SC-12164	1:100	PBS, 10%FBS, 0.01% Triton X-100
Rabbit IgG AF594	Donkey	IgG	A21207	1:500	PBS, 10%FBS, 0.01% Triton X-100
Mouse IgG AF647	Donkey	IgG	A32787	1:500	PBS, 10%FBS, 0.01% Triton X-100

Supplementary Table 3 Walked design of candidate siRNAs for selective silencing of *NRAS* c.181A>C

siRNA	Sense (+TT overhang)	Antisense (+TT overhang)	mRNA complementarity
siRNA1	AUACUGGAUACAGCUGGAATT	UUCCAGCUGUAUCCAGUAUTT	*NRAS* c.163-181
siRNA2	UACUGGAUACAGCUGGAAATT	UUUCCAGCUGUAUCCAGUATT	*NRAS* c.164-182
siRNA3	ACUGGAUACAGCUGGAAAATT	UUUUCCAGCUGUAUCCAGUTT	*NRAS* c.165-183
siRNA4	CUGGAUACAGCUGGAAAAGTT	CUUUUCCAGCUGUAUCCAGTT	*NRAS* c.166-184
siRNA5	UGGAUACAGCUGGAAAAGATT	UCUUUUCCAGCUGUAUCCATT	*NRAS* c.167-185
siRNA6	GGAUACAGCUGGAAAAGAATT	UUCUUUUCCAGCUGUAUCCTT	*NRAS* c.168-186
siRNA7	GAUACAGCUGGAAAAGAAGTT	CUUCUUUUCCAGCUGUAUCTT	*NRAS* c.169-187
siRNA8	AUACAGCUGGAAAAGAAGATT	UCUUCUUUUCCAGCUGUAUTT	*NRAS* c.170-188
siRNA9	UACAGCUGGAAAAGAAGAGTT	CUCUUCUUUUCCAGCUGUATT	*NRAS* c.171-189
siRNA10	ACAGCUGGAAAAGAAGAGUTT	ACUCUUCUUUUCCAGCUGUTT	*NRAS* c.172-190
siRNA11	CAGCUGGAAAAGAAGAGUATT	UACUCUUCUUUUCCAGCUGTT	*NRAS* c.173-191
siRNA12	AGCUGGAAAAGAAGAGUACTT	GUACUCUUCUUUUCCAGCUTT	*NRAS* c.174-192
siRNA13	GCUGGAAAAGAAGAGUACATT	UGUACUCUUCUUUUCCAGCTT	*NRAS* c.175-193
siRNA14	CUGGAAAAGAAGAGUACAGTT	CUGUACUCUUCUUUUCCAGTT	*NRAS* c.176-194
siRNA15	UGGAAAAGAAGAGUACAGUTT	ACUGUACUCUUCUUUUCCATT	*NRAS* c.177-195
siRNA16	GGAAAAGAAGAGUACAGUGTT	CACUGUACUCUUCUUUUCCTT	*NRAS* c.178-196
siRNA17	GAAAAGAAGAGUACAGUGCTT	GCACUGUACUCUUCUUUUCTT	*NRAS* c.179-197
siRNA18	AAAAGAAGAGUACAGUGCCTT	GGCACUGUACUCUUCUUUUTT	*NRAS* c.180-198
siRNA19	AAAGAAGAGUACAGUGCCATT	UGGCACUGUACUCUUCUUUTT	*NRAS* c.181-199

Supplementary Table 4 Gene expression assays

Species	Gene	Type	Code / Forward	Reverse
Human	*NRAS (WT)*	Primers	CATACTGGATACAGCTGGAC	TTGATGGCAAATACACAGAGGA
Human	*NRAS (c.181C>A; p.(Q61K)*	Primers	CATACTGGATACAGCTGGAA	TTGATGGCAAATACACAGAGGA
Human	*GAPDH*	Primers	CAATGACCCCTTCATTGACC	AATTTGCCATGGGTGGAAT
Human	*ARL6IP1*	Taqman	ThermoFisher, Hs00760013_s1	NA
Human	*ERN1*	Taqman	ThermoFisher, Hs00980095_m1	NA
Human	*BIRC5*	Taqman	ThermoFisher, Hs04194392_s1	NA
Human	*GAPDH*	Taqman	ThermoFisher, Hs02786624_g1	NA
Mouse	*Nras*	Primers	GGACAGTTGACACAAAGCAAGCC	TGGCGTATCTCCCTTACCAGTG
Mouse	*Gapdh*	Primers	CATCACTGCCACCCAGAAGACTG	ATGCCAGTGAGCTTCCCGTTCAG
Mouse	*Arl6ip1*	Taqman	ThermoFisher, Mm01274634_m1	NA
Mouse	*Gapdh*	Taqman	ThermoFisher, Mm99999915_g1	NA

Supplementary Table 5 Antibodies used for western blotting.

Target	Species	Type	Code	Dilution	Blocking
Total ERK	Mouse	IgG	CST-9107	1:1000	TBS, 5% fish gelatin, 0.1% Tween-20
pERK	Rabbit	IgG	CST-4377	1:1000	TBS, 5% fish gelatin, 0.1% Tween-20
NRAS	Mouse	IgG	SC-31	1:100	TBS, 3% BSA, 0.1% Tween-20
Vinculin	Mouse	IgG1	MA5-11890	1:5000	TBS, 3% BSA, 0.1% Tween-20
Mouse IgG HRP	Goat	IgG	P-0447	1:5000	TBS, 0.1% Tween-20
Rabbit IgG HRP	Goat	IgG	P-0448	1:5000	TBS, 0.1% Tween-20
Mouse IgG IRDye 680RD	Goat	IgG	926-68071	1:7000	TBS, 0.1% Tween-20
Rabbit IgG IRDye 800CW	Goat	IgG	926-32210	1:10000	TBS, 0.1% Tween-20

Supplementary Video Legends

Supplementary Video 1 Abnormal mitosis in patient-derived naevus cells. Example of abnormal mitosis event whereby a single naevus cell produces three daughter cells. Frame / 10 minutes.

Supplementary Data File Legends

Supplementary Data 1 Enriched GO terms from RNAseq data (HCT116 cells). GO term enrichment following 48 hour treatment of HCT116 $NRAS^{WT}$ cells with siRNA1 (sheet 1), siRNA8 (sheet 2), siRNA15 (sheet 3); HCT116 $NRAS^{Q61K}$ cells with siRNA1 (sheet 4), siRNA8 (sheet 5), siRNA15 (sheet 6). The GO terms listed were returned from Metascape following input of genes differentially expressed (adjusted $p \leq 0.05$; 2 fold change) in the given conditions.

Supplementary Data 2 Enriched GO terms from RNAseq data (Naevus cells). GO term enrichment following 48 hour treatment of naevus cells with $siNRAS^{Q61K}$. Terms returned from Metascape following input of genes differentially expressed (adjusted $p \leq 0.05$; 1 fold change).